J Hum Genet (2008) 53:515–523
DOI 10.1007/s10038-008-0279-x

ORIGINAL ARTICLE

Global correlation analysis for micro-RNA and mRNA expression profiles in human cell lines

Yoshinao Ruike · Atsuhiko Ichimura · Soken Tsuchiya · Kazuharu Shimizu · Ryo Kunimoto · Yasushi Okuno · Gozoh Tsujimoto

Received: 19 February 2008 / Accepted: 29 February 2008 / Published online: 10 May 2008

Abstract Microribonucleic acids (miRNAs) are small noncoding RNAs that negatively regulate gene expression at the posttranscriptional level. Although considerable progress has been made in studying the function of miRNAs, they still remain largely unclear, mainly because of the difficulty in identifying target genes for miRNA. We performed a global analysis of both miRNAs and mRNAs expression across 16 human cell lines and extracted negatively correlated pairs of miRNA and mRNA which indicate miRNA-target relationship. The many of known-target of *miR-124a* showed negative correlation, suggesting our analysis were valid. We further extracted physically relevant miRNA-target gene pairs, applying computational target prediction algorithm with inverse correlations of miRNA and messenger RNA (mRNA) expression. Furthermore, gene-ontology-based annotation and functional enrichment analysis of the extracted miRNA-target gene pairs made it possible to indicate putative functions of miRNAs. The data collected here will be of value for further studies into the function of miRNA.

Keywords Micro-RNA · Microarray · Transcriptome · Correlation analysis · GO analysis

Electronic supplementary material The online version of this article (doi:10.1007/s10038-008-0279-x) contains supplementary material, which is available to authorized users.

Y. Ruike · A. Ichimura · R. Kunimoto · G. Tsujimoto (✉)
Department of Genomic Drug Discovery Science,
Graduate School of Pharmaceutical Sciences,
Kyoto University, 46-29 Yoshida Shimoadachi-cho Sakyo-ku,
Kyoto 606-8501, Japan
e-mail: gtsuji@pharm.kyoto-u.ac.jp

S. Tsuchiya · K. Shimizu
Department of Nanobio Drug Discovery,
Graduate School of Pharmaceutical Sciences,
Kyoto University, Kyoto, Japan

Y. Okuno
Department of Pharmacoinformatics,
Graduate School of Pharmaceutical Sciences,
Kyoto University, Kyoto, Japan

Introduction

Microribonucleic acids (miRNAs) are a class of small (approximately 22 nucleotides) noncoding RNAs that negatively regulate gene expression at the posttranscriptional level. They play profound and pervasive roles in manipulating gene expression involved in cell development, proliferation and apoptosis in various eukaryotes (Sevignani et al. 2006). Also, recent evidence indicated that aberrant miRNA expression in the pathogenesis of several human diseases (van Rooij et al. 2006; Takamizawa et al. 2004; Iorio et al. 2005), revealing that miRNA genes could be a potential target for drug discovery (Sevignani et al. 2006; Liu et al. 2007; Tsuchiya et al. 2006).

In the past few years, several hundred miRNAs were identified in animals and plants, although it is estimated that miRNAs account for ~1% of predicted genes in higher eukaryotic genomes (Griffiths-Jones 2004). Only a handful of miRNA, however, have been functionally characterized. These findings, together with the complicated expression patterns and large number of predicted targets, imply that miRNAs may regulate a broad range of physiological and developmental process.

Idnetifying targets of each miRNA is crucial for understanding the biological functions of miRNAs, as miRNA-directed regulation occurs at a posttranscriptional level via interaction with their target messenger RNA (mRNA)

to elicit degradation or translational repression of complementary mRNA targets (Behm-Ansmant et al. 2006; Chendrimada et al. 2007). Also, miRNAs are known to be only partially complementary to their targets and can induce significant degradation of many mRNA targets in animals (Bagga et al. 2005; Jing et al. 2005; Giraldez et al. 2006; Rehwinkel et al. 2006). This ambiguity makes it difficult to predict the targets of miRNAs [up to 30% of genes have been predicted to be regulated by miRNAs (Lewis et al. 2003)]. However, most of the predicted miRNA-target pairs remain to be biologically verified, because a simple, high throughput method to biologically validate miRNA-targets does not exist. Several recent studies revealed spatial or temporal avoidance of miRNA coexpression with target genes (Farh et al. 2005; Sood et al. 2006). Thus, genes preferentially expressed at the same time and place as an miRNA have evolved to selectively avoid sites matching the miRNA (Farh et al. 2005). These findings may support the negative correlation between miRNA and their target mRNA expression level as a whole. Based on the idea that negative correlation between miRNA and mRNA expression levels may reflect miRNA-target relationship, we performed a global analysis of both miRNA and mRNA expression across 16 human cell lines. Global correlation analysis of the expression profiles collected revealed a useful approach to identify the miRNA-target interactions.

Materials and methods

Cell lines and RNA purification

We used 16 well-studied, various organ-derived cell lines in this study: human lung carcinoma A549 (Giard et al. 1973), fibrosarcoma HT1080 (Rasheed et al. 1974), cervix carcinoma Henrietta Lacks (HeLa) (Scherer et al. 1953), cervix carcinoma HeLaS3 (subclone of HeLa) (Puck et al. 1956), hepatocellular carcinoma Huh7 (Nakabayashi et al. 1985), breast adenocarcinoma MCF7 (Soule et al. 1973), breast adenocarcinoma MDAMB231 (Cailleau et al. 1974), embryonal kidney HEK293T (subclone of HEK293) (DuBridge et al. 1987), colon adenocarcinoma HT29 (Fogh et al. 1977), hepatocellular carcinoma HepG2 (Aden et al. 1979), neuroblastoma SKNMC (Biedler et al. 1973), colon adenocarcinoma $Caco_2$ (Fogh et al. 1977), embryonal kidney HEK293 (Graham et al. 1977), and colon carcinoma HCT116 (Brattain et al. 1981). Cells were cultured in Dulbecco's modified Eagle's medium (DMEM) containing 10% fetal bovine serum (FBS). Human T-cell lukemia Jurkat (Schneider et al. 1977) and chronic myeloid leukemia K562 (Lozzio and Lozzio 1973) cell lines were cultured in Roswell Park Memorial Institute (RPMI) medium containing 10% FBS. Exponentially growing cells were harvested, and total RNA was collected by standard procedures using ISOGEN (Nippon Gene) and chloroform and precipitated with isopropanol. Integrity and purity of RNA was verified with an Agilent Bioanalyzer.

Quantification of miRNAs using stem-loop real-time PCR

Expression of 148 miRNAs was measured by reverse transcription followed by the real-time polymerase chain reaction (RT-PCR) assay as previously described (Gaur et al. 2007). This method uses stem-loop primers for reverse transcription followed by RT-PCR (TaqMan MicroRNA Assays; Applied Biosystems). ABI PRISM™ 7700 Sequence Detector was used to detect amplification. This stem-loop RT-PCR method detects specifically mature, but not precursor, miRNA. RNA input was normalized by measuring U6 expression using the following TaqMan probes.

5′FAM-CCCCTGCGCAAGGA-MGB3′, forward primer: 5′-TGGAACGATACAGAGAAGATTAGCA-3′, reverse primer: 5′-AACGCTTCACGAATTTGCGT-3′. Expression data of a few miRNA was confirmed to be well correlated to those obtained by Northern analysis (data not shown).

Microarray experiments

Genome-wide mRNA expression profiles of 16 human cell lines were obtained by microarray analysis with the Affymetrix GeneChip Human Genome U133 Plus 2.0 Array, according to the manufacturer's instructions. Briefly, double-stranded complementary DNA (cDNA) was synthesized from total RNA. An in vitro transcription reaction was then carried out to produce biotin-labeled complementary RNA (cRNA) from the cDNA. The cRNA was then fragmented and used for hybridization. The hybridized probe array was subsequently stained and scanned by a Genechip Scanner 3000. We used the robust multiarray analysis (RMA) expression measure that represents the log transform of (background corrected and normalized) intensities of the GeneChips (Gautier et al. 2004). RMA measures were computed using the R package program (http://www.bioconductor.org). The probe sets with the lowest maximal expression across the samples in the data set (30%) were removed.

Data analysis

Experimentally normalized ΔCt values for the miRNA profiles, or normalized microarray data sets for mRNA profiles, were used to classify cells by agglomerative hierarchical clustering based on Euclidean distances between data sets. The ΔCt values for the miRNA profiles

were used to evaluate the 16 cell lines by agglomerative hierarchical clustering using average linkage and correlation similarity and verified for significance by multiscale bootstrap resampling analysis (Suzuki and Shimodaira 2006). Classical Pearson's correlation tests were performed to verify the relationships between expression profiles of miRNA and mRNA. The significance of each correlation was assessed by assuming that the distribution of correlations under the null hypothesis of no correlation follows a t distribution with $n - 2$ degrees of freedom, where n is the number of measurements in the expression profile.

Target prediction and GO term enrichment analysis

Potential targets for miRNAs were predicted among 3′ untranslated region (UTR) sequences of inversely correlated target transcripts using the miRanda algorithm, which is associated with the Sanger MIRBASE (Enright et al. 2003). algorithm parameters were set as follows: score threshold at 50, energy threshold at −20 kcal/mol, scaling parameter at 4, gap-open penalty at −2, and gap-extend penalty at −8. The significance of enrichment of a list of target genes with genes belonging to a gene ontology (GO) group were scored using weight algorithm (Ashburner et al. 2000; Alexa et al. 2006). The algorithm for GO group scoring was implemented in the R programming language. The results were obtained using R version 2.5.0 and the libraries provided by the Bioconductor project, version 1.14 (Gentleman et al. 2004).

Results

Micro-RNA expression profiles in 16 human cell lines

We performed quantitative measurement of 155 kinds of mature human miRNAs in 16 human cell lines. The probe sets for miRNA with minimal Ct values >35 in all cell lines were excluded from the following analysis. Seven miRNAs were thus excluded, and the remaining 148 different mature miRNAs were used for further analysis (expression data in a text format is provided in Table S1).

To characterize the expression patterns of miRNAs, hierarchical clustering was performed using normalized ΔCt values (Fig. 1). The most prominent feature of the clustered data was that many miRNAs displayed similar expression pattern among the majority of samples, although some miRNAs displayed very specific expression patterns. Hierarchical clustering of 16 cell lines resulted in a dendrogram, which contained small clusters reflecting common tissue origin (e.g., HepG2 and Huh7) or subclones (e.g., HeLa and HeLaS3). We also found some cell lines showed characteristic expression patterns independent of their tissue origins. In particular, $Caco_2$ had a very different expression pattern from HT-29 or HCT-116, although all of them originated from colon carcinoma. Thus, some miRNAs were specifically expressed in $Caco_2$ (e.g., miR-372 and -373), but not in either HT-29 or HCT-116. Determining the differential expression of miRNAs from similar biological backgrounds would be of value to investigate the functions of miRNA.

To classify expression patterns of miRNAs, we employed hierarchical clustering based on correlation similarity between each miRNA (Fig. 2). This analysis revealed the relationships between miRNAs that had similar expression patterns among cell lines. To assess the robustness of these relationships, we conducted a multiscale bootstrap resampling anaysis (Suzuki and Shimodaira 2006) and verified the significance (Fig. 2). The resulting dendrogram had several statistically significant clusters of miRNAs, suggesting that their expression might be commonly regulated. Noticeably, many miRNAs that coexpressed formed genomic clusters. Frequent coexpression between neighboring miRNAs that formed genomic clusters were previously reported, analyzing miRNA expression patterns across 24 normal human organs (Baskerville and Bartel 2005). To test coexpression between neighboring miRNAs, we examined the relationship between genomic distance and correlation coefficients between neighboring miRNAs. Among the miRNAs measured, miRNAs with several genomic origins, which can be indicated by the presence of multiple premature miRNA, were excluded in the following analysis. Micro-RNAs from the same chromosome and oriented in the same direction were defined as "paired". For the resulting 224 pairs (miRNA pairs are summarized in Table S2), we examined the relationship between the genomic distance of each miRNA pair and the correlation coefficient of the miRNA expression pattern (Fig. 3). Most pairs of miRNAs separated by <100 kb showed highly positive correlation.

Genome-wide gene expression analysis

Next, we obtained a global gene expression profile by employing microarray analysis using the same RNA samples used for quantifying miRNA (microarray data was deposited in Gene Expression Omnibus accession number GSE10021). The miRNAs located in the intronic region of genes are usually coordinately expressed with their host gene mRNA (Baskerville and Bartel 2005). Among 148 miRNAs measured in this study, 40 were derived from the intronic region of genes and examined for their correlation with the corresponding host genes

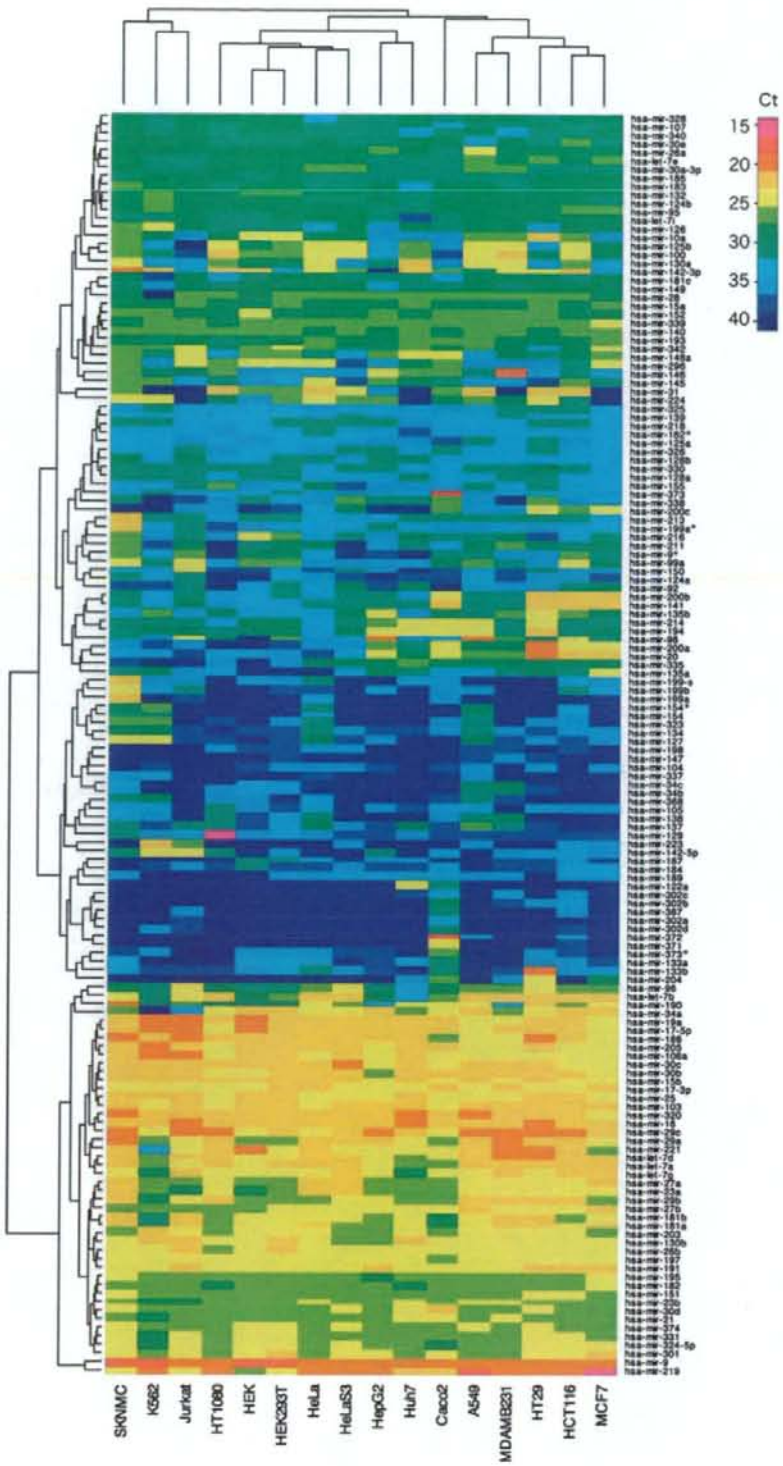

Fig. 1 Hierarchical clustering of 148 microribonucleic acid (miRNA) expression profiles in 16 human cell lines. Expression profiles (ΔCt values) of 148 miRNAs measured in total RNA from cell lines were clustered

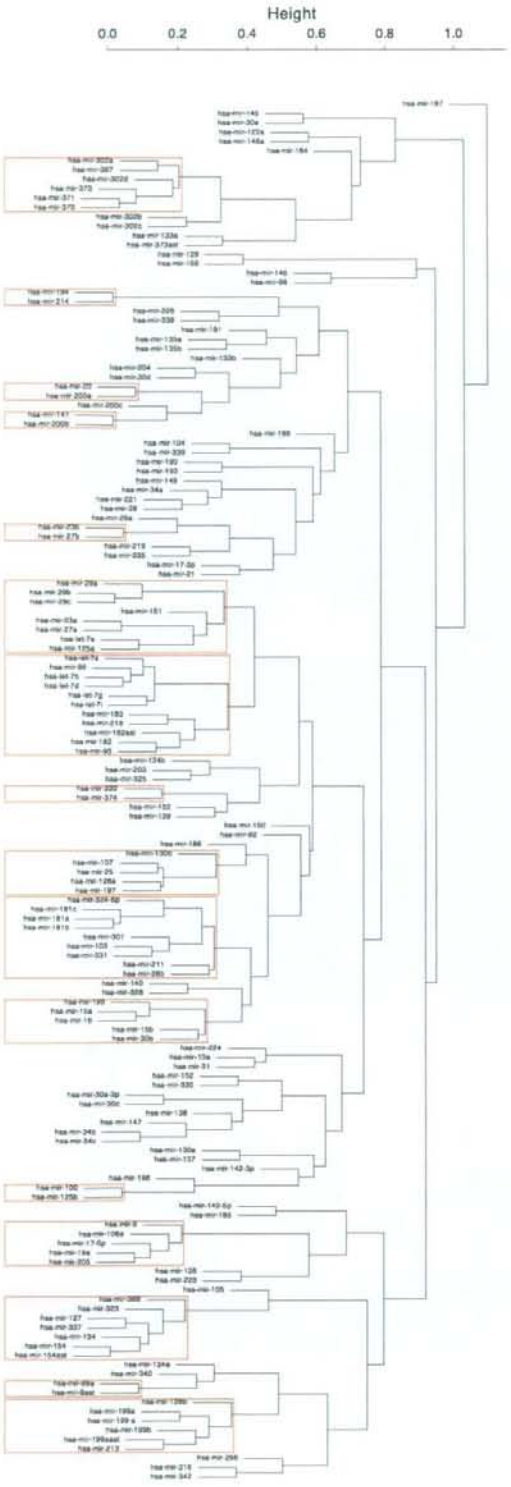

Fig. 2 Hierarchical clustering with bootstrap analysis based on correlational expression profiles among 148 microribonucleic acids (miRNAs). Expression profiles of 148 miRNAs were clustered and verified for significance by multiscale bootstrap resampling analysis (1,000 iterations, sampling with replacement). Clusters were scored as statistically significant in cases in which miRNAs clustered with a 99% or better confidence interval (corresponding to $p < 0.01$), as determined by the bootstrap analysis

using standard Pearson's correlation test (Table 1). The strong correlation between intronic miRNA and host genes was observed, suggesting they are derived from the same precursor genes, which might be under the control of the same promoter.

To determine whether the negative correlation observed between miRNA and gene expression reflected miRNA-target gene relationships, we first examined the relationship using a previously identified miRNA-target gene pairs. We examined *miR-124a*, which has the largest number of known target genes (Lim et al. 2005), as a control. The *miR-124a* expression level measured by RT-PCR analysis was compared with either those of the known target genes or those of all genes, both obtained by microarray analysis in 16 cell lines. Then, each data set was subjected to Pearson's correlation test (Fig. 4). The distribution of correlation coefficient for *miR-124a*-target gene pairs was shifted toward negative side, compared to that of the *miR-124a*-total gene pairs. The mean of correlation coefficients between the two sets was significantly different ($p < 0.01$). Furthermore, Fisher's exact test showed a significant accumulation of target genes

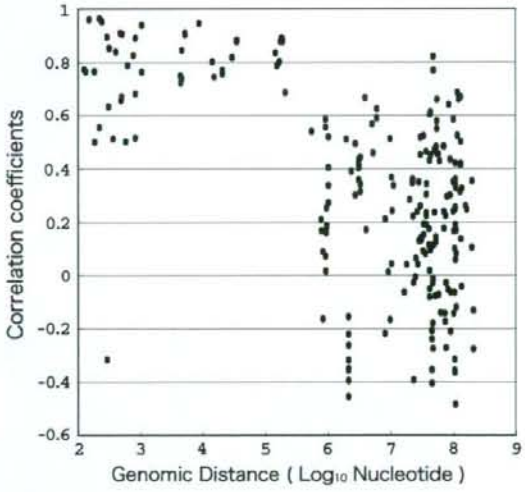

Fig. 3 Relationship between the distance separating mico-RNA (miRNA) loci and their coordinate expression in human tissues. Each miRNA was paired with each of the others lying in the same orientation on the same chromosome. For each pair, the correlation coefficient for their expression was plotted according to the distance between the two loci (*white circle*)

Table 1 Correlation of intronic microribonucleic acid (miRNA) expression with host gene expression

Host gene	RefSeq ID	miRNA	Correlation
MEST	NM_002402	hsa-mir-335	0.92
C9orf3	NM_032823	hsa-mir-23b	0.86
EVL	NM_016337	hsa-mir-342	0.84
C9orf3	NM_032823	hsa-mir-27b	0.83
PTK2	NM_005607	hsa-mir-151	0.82
240284_x_at	–	hsa-mir-141	0.80
GABRE	NM_004961	hsa-mir-224	0.78
RNF130	NM_018434	hsa-mir-340	0.77
EGFL7	NM_016215	hsa-mir-126	0.76
LPP	NM_005578	hsa-mir-28	0.72
229934_at	–	hsa-mir-223	0.70
1554097_a_at	–	hsa-mir-31	0.67
ZNF265	NM_005455	hsa-mir-186	0.66
FAM33A	NM_182620	hsa-mir-301	0.66
EML2	NM_012155	hsa-mir-330	0.60
1558515_at	–	hsa-mir-374	0.60
GPC1	NM_002081	hsa-mir-149	0.59
MGC11257	NM_032350	hsa-mir-339	0.59
C9orf3	NM_032823	hsa-mir-189	0.59
ARPP-21	NM_001025068	hsa-mir-128b	0.58
BIC	NR_001458	hsa-mir-155	0.58
240284_x_at	–	hsa-mir-200c	0.56
AATK	XM_927215	hsa-mir-338	0.54
FSTL1	NM_007085	hsa-mir-198	0.53
SMC4L1	NM_001002799	hsa-mir-15b	0.52
CTDSP1	NM_021198	hsa-mir-26b	0.50
MCM7	NM_005916	hsa-mir-25	0.50
MEG3	NR_002766	hsa-mir-127	0.45
ARRB1	NM_004041	hsa-mir-326	0.39
PDE2A	NM_002599	hsa-mir-139	0.26
TMEM113	NM_025222	hsa-let-7g	0.26
228528_at	–	hsa-mir-29c	0.21
WWP2	NM_007014	hsa-mir-140	0.19
TLN2	NM_015059	hsa-mir-190	0.16
R3HDM1	NM_015361	hsa-mir-128a	0.15
TRPM3	NM_001007470	hsa-mir-204	0.00
COPZ2	NM_016429	hsa-mir-152	−0.10
PANK1	NM_138316	hsa-mir-107	−0.14
DLEU2	NR_002612	hsa-mir-15a	−0.17
C21orf34	NM_001005732	hsa-mir-99a	−0.38

Gene symbol of the host gene, RefSeq ID, intronic miRNA, and correlation coefficient are listed for each intronic miRNA host gene pairs

within the inversely correlated group of genes [odds ratio (OR) 2.5, $p < 0.01$], indicating that the negative correlation observed between miRNA and gene expression in this reflects miRNA-target gene relationship.

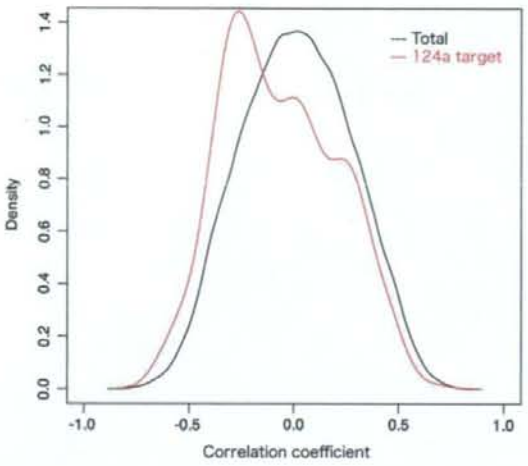

Fig. 4 Distribution of correlation coefficients between *miR-124a* and known targets of *miR-124a*. The estimated densities of distributions for target genes (*red*) or total genes (*black*) were plotted

To extract a global relationship of miRNA-target genes, all miRNA-mRNA pairs were subjected to Pearson's correlation test. Of the total 5.7 million different pairs examined, 184,901 miRNA-mRNA pairs (3.2%) showed a negative correlation.

Applying miRNA-target prediction algorithm

Because negative correlation might also reflect indirect regulation of gene expression by miRNAs, we further examined whether the extracted genes contained the corresponding target sites for miRNA in the 3′ UTRs. To seek miRNA-directed target sites, we adopted the miRanda algorithm (Enright et al. 2003) to a set of 30,664 different transcripts enrolled in RefSeq and monitored them by microarray. This analysis yielded 44,572 miRNA-target gene pairs that fulfilled the conditions that the expression level of genes negatively correlated with that of the miRNA, and that the genes contain the target sequence against the miRNA. Hence, approximately 300 genes per miRNA were extracted on average. Based on the extracted miRNA-target gene pairs, we next tried to predict the functions of miRNA. Thus, we calculated the frequency of gene ontology (GO) term (biological process area) of target genes for each miRNA. The GO terms were chosen if the frequency of the GO term was statistically significantly more than that expected by chance. Table 2 lists the top 30 miRNAs that had the highest GO term frequency. Most miRNA-target gene pairs were found to be novel, and the frequently noted GO terms for each miRNA was a diverse and wide variety in the biological process.

Table 2 Gene ontology (GO) term enrichment analysis for predicted microribonucleic acid (miRNA)-target genes

GO ID	Number of categorized genes	Number of extracted genes	Number of expected genes	*P* value (weight algorithm)	miRNA	GO definition
GO:0006694	139	10	1.1	1.70E-07	hsa-mir-320	Steroid biosynthesis
GO:0006694	139	8	0.79	1.30E-06	hsa-mir-34c	Steroid biosynthesis
GO:0016125	158	9	1.19	3.20E-06	hsa-mir-34b	Sterol metabolism
GO:0030001	663	27	10.95	1.80E-05	hsa-mir-331	Metal ion transport
GO:0006955	991	42	19.2	2.00E-05	hsa-mir-296	Immune response
GO:0045086	19	5	0.36	2.20E-05	hsa-mir-34a	Positive regulation of interleukin-2 biosynthesis
GO:0046321	9	3	0.06	2.40E-05	hsa-mir-99a	Positive regulation of fatty acid oxidation
GO:0015808	4	2	0.01	3.60E-05	hsa-mir-195	L-alanine transport
GO:0001568	369	12	2.95	4.50E-05	hsa-mir-150	Blood-vessel development
GO:0001678	4	2	0.01	7.10E-05	hsa-mir-16	Cell glucose homeostasis
GO:0042104	12	4	0.25	8.20E-05	hsa-mir-324-5p	Positive regulation of activated T-cell proliferation
GO:0016125	158	5	0.44	8.40E-05	hsa-mir-152	Sterol metabolism
GO:0006694	139	7	1.04	8.90E-05	hsa-mir-34b	Steroid biosynthesis
GO:0051085	19	4	0.25	9.70E-05	hsa-mir-133a	Chaperone cofactor-dependent protein folding
GO:0007588	78	9	1.92	0.00013	hsa-mir-328	Excretion
GO:0046006	16	4	0.3	0.00018	hsa-mir-149	Regulation of activated T-cell proliferation
GO:0045471	4	2	0.02	0.00019	hsa-mir-148a	Response to ethanol
GO:0006355	4315	42	24.64	0.00019	hsa-mir-31	Regulation of transcription, DNA dependent
GO:0006955	991	29	13.02	0.00022	hsa-mir-133a	Immune response
GO:0006656	14	2	0.02	0.00026	hsa-mir-368	Phosphatidylcholine biosynthesis
GO:0042552	44	2	0.03	0.00028	hsa-mir-29c	Myelination
GO:0030001	663	33	16.34	0.0003	hsa-mir-328	Metal ion transport
GO:0042104	12	3	0.14	0.00032	hsa-mir-181b	Positive regulation of activated T-cell proliferation
GO:0006825	16	3	0.14	0.00033	hsa-let-7i	Copper ion transport
GO:0006857	14	3	0.14	0.00033	hsa-mir-122a	Oligopeptide transport
GO:0006611	54	3	0.13	0.00033	hsa-mir-21	Protein export from nucleus
GO:0006825	16	3	0.14	0.00034	hsa-mir-132	Copper ion transport
GO:0030041	71	4	0.33	0.00035	hsa-mir-154	Actin filament polymerization
GO:0006235	3	2	0.03	0.00035	hsa-mir-27b	dTTP biosynthesis
GO:0006011	4	2	0.03	0.00035	hsa-mir-325	UDP-glucose metabolism

Top 30 highly enriched GO terms. *P* values were calculated using weight algorithm

Discussion

To investigate biological functions of miRNA, it is critical to identify miRNA-directed target genes. However, currently available computational methods (e.g., miRanda, PicTar, and TargetScan) predict numerous target genes that contain many false positives for miRNA (Mazière and Enright 2007). Also, experimental verification of miRNA-target relationship is complicated by the potential outcome of such an interaction being either translational repression or degradation. Furthermore, miRNAs can target multiple genes, and thereby the biological function of a single miRNA can be diverse. Hence, not only to achieve a higher degree of specificity of the prediction (few false positives) but also to comprehensively understand the function of miRNA, large-scale prediction of targets across a whole genome would be required.

In this study, we intended to investigate global miRNA-target relationships, assuming a negative correlation between miRNA and gene expression levels as an indicator for the miRNA-target relationship. The collected genome-wide expression data sets of both miRNA and mRNA enabled global correlation analysis between an miRNA and its target gene. Based on the observation that the expression of genes known as *miR-124a* targets tended to be negatively correlated with *miR-124a* expression, we reasoned that correlation analysis would be useful in investigating miRNA-target relationship. Then, we further extracted miRNA-target gene pairs by collecting genes that contain miRNA-directed target sites within 3′ UTR. The resulting list of miRNA gene pairs may provide useful information in investigating miRNA-target relationship.

Our miRNA-expression study provides important information on endogenous miRNA expression in 16 cell lines. One of the most serious problems in exploring miRNA function in a cell-base assay is the influence of endogenous miRNA expression. For example, in vitro reporter gene assay, a general approach used for target gene validation, has different results in different cell lines examined. This is thought to be due to the differential expression of endogenous miRNAs in the cell line used, as it strongly affects background expression of the reporter gene containing the test sequence. As we examined genetically tractable and well-studied cell lines in this study, the data obtained should be informative for studying functions of miRNA using those cell lines.

In collecting global miRNA and gene-expression profiles, we observed that many of the neighboring miRNA pairs, which were located within ~100-kb region of the chromosome, showed a significantly positive correlation and that the expression of intronic miRNAs was generally correlated with that of host genes. These results were consistent with the idea that clustered miRNAs are processed from the same primary transcript (Suh et al. 2004) and that intronic miRNAs are from the same primary transcript as their host gene (Lau et al. 2001; Sempere et al. 2004). Unexpectedly, however, we observed that miRNAs expressed from the same miRNA precursor (ex, *miR-142-3*p and *-5p*) were not coexpressed. This discrepancy could be explained by the fact that expression of these miRNAs depends on asymmetric selection of mature miRNA strand followed by the cleavage of pre-miRNA (Hutvagner 2005). Although it likely involves differential binding to and then differential retention of the two individual RNA strands by Dicer and its associated proteins (Zeng 2006), the detailed molecular mechanism for this asymmetry is not clear. The differential expression among cell lines we studied may provide a clue to the mechanism of asymmetric selectivity.

Correlated expression of miRNA and corresponding genes may imply their association in function as well. GO-based annotation and functional enrichment analysis of the extracted miRNA-target gene pairs made it possible to indicate putative functions of miRNAs. The approach developed in this study should be of value for future studies into the functions of miRNAs.

Acknowledgments This work was supported in part by research grants from the Scientific Fund of the Ministry of Education, Science, and Culture of Japan (to GT); National Institute of Biomedical Innovation (to GT); the Program for Promotion of Fundamental Studies in Health Sciences of the National Institute of Biomedical Innovation (NIBIO) (to GT); the Japan Health Science Foundation and the Ministry of Human Health and Welfare (to GT); and the 21st Century Center of Excellence Program "Knowledge Information Infrastructure for Genome Science" (to GT and YR). YR is supported as a Research Assistant by 21st Century COE program "Knowledge Information Infrastructure for Genome Science".

References

Aden DP, Fogel A, Plotkin S, Damjanov I, Knowles BB (1979) Controlled synthesis of HBsAg in a differentiated human liver carcinoma-derived cell line. Nature 282:615–616

Alexa A, Rahnenführer J, Lengauer T (2006) Improved scoring of functional groups from gene expression data by decorrelating GO graph structure. Bioinformatics 22:1600–1607

Ashburner M, Ball CA, Blake JA, Botstein D, Butler H, Cherry JM, Davis AP, Dolinski K, Dwight SS, Eppig JT, Harris MA, Hill DP, Issel-Tarver L, Kasarskis A, Lewis S, Matese JC, Richardson JE, Ringwald M, Rubin GM, Sherlock G (2000) Gene ontology: tool for the unification of biology. The gene ontology consortium. Nat Genet 25:25–29

Bagga S, Bracht J, Hunter S, Massirer K, Holtz J, Eachus R, Pasquinelli AE (2005) Regulation by let-7 and lin-4 miRNAs results in target mRNA degradation. Cell 122: 553–563

Baskerville S, Bartel DP (2005) Microarray profiling of microRNAs reveals frequent coexpression with neighboring miRNAs and host genes. RNA 11:241–247

Behm-Ansmant I, Rehwinkel J, Doerks T, Stark A, Bork P, Izaurralde E (2006) mRNA degradation by miRNAs and GW182 requires both CCR4:NOT deadenylase and DCP1:DCP2 decapping complexes. Genes Dev 20:1885–1898

Biedler JL, Helson L, Spengler BA (1973) Morphology and growth, tumorigenicity, and cytogenetics of human neuroblastoma cells in continuous culture. Cancer Res 33:2643–2652

Brattain MG, Fine WD, Khaled FM, Thompson J, Brattain DE (1981) Heterogeneity of malignant cells from a human colonic carcinoma. Cancer Res 41:1751–1756

Cailleau R, Young R, Olivè M, Reeves WJ (1974) Breast tumor cell lines from pleural effusions. J Natl Cancer Inst 53:661–674

Chendrimada TP, Finn KJ, Ji X, Baillat D, Gregory RI, Liebhaber SA, Pasquinelli AE, Shiekhattar R (2007) MicroRNA silencing through RISC recruitment of eIF6. Nature 447:823–828

DuBridge RB, Tang P, Hsia HC, Leong PM, Miller JH, Calos MP (1987) Analysis of mutation in human cells by using an Epstein–Barr virus shuttle system. Mol Cell Biol 7:379–387

Enright AJ, John B, Gaul U, Tuschl T, Sander C, Marks DS (2003) MicroRNA targets in Drosophila. Genome Biol 5:R1

Farh KK, Grimson A, Jan C, Lewis BP, Johnston WK, Lim LP, Burge CB, Bartel DP (2005) The widespread impact of mammalian

MicroRNAs on mRNA repression and evolution. Science 310:1817–1821

Fogh J, Wright WC, Loveless JD (1977) Absence of HeLa cell contamination in 169 cell lines derived from human tumors. J Natl Cancer Inst 58:209–214

Gaur A, Jewell DA, Liang Y, Ridzon D, Moore JH, Chen C, Ambros VR, Israel MA (2007) Characterization of microRNA expression levels and their biological correlates in human cancer cell lines. Cancer Res 67:2456–2468

Gautier L, Cope L, Bolstad BM, Irizarry RA (2004) Affy–analysis of Affymetrix GeneChip data at the probe level. Bioinformatics 20:307–315

Gentleman RC, Carey VJ, Bates DM, Bolstad B, Dettling M, Dudoit S, Ellis B, Gautier L, Ge Y, Gentry J, Hornil K, Hothorn T, Huber W, Iacus S, Irizarry R, Leisch F, Li C, Maechler M, Rossini AJ, SawitzkiG, Smith C, Smyth G, Tierney L, Yang JY, Zhang J (2004) Bioconductor: open software development for computational biology and bioinformatics. Genome Biol 5:R80

Giard DJ, Aaronson SA, Todaro GJ, Arnstein P, Kersey JH, Dosik H, Parks WP (1973) In vitro cultivation of human tumors: establishment of cell lines derived from a series of solid tumors. J Natl Cancer Inst 51:1417–1423

Giraldez AJ, Mishima Y, Rihel J, Grocock RJ, VanDongen S, Inoue K, Enright AJ, Schier AF (2006) Zebrafish MiR-430 promotes deadenylation and clearance of maternal mRNAs. Science 312:75–79

Graham FL, Smiley J, Russell WC, Nairn R (1977) Characteristics of a human cell line transformed by DNA from human adenovirus type 5. J Gen Virol 36:59–74

Griffiths-Jones S (2004) The microRNA registry. Nucleic Acids Res 32:D109–D111

Hutvagner G (2005) Small RNA asymmetry in RNAi: function in RISC assembly and gene regulation. FEBS Lett 579:5850–5857

Iorio MV, Ferracin M, Liu CG, Veronese A, Spizzo R, Sabbioni S, Magri E, Pedriali M, Fabbri M, Campiglio M, Mènard S, Palazzo JP, Rosenberg A, Musiani P, Volinia S, Nenci I, Calin GA, Querzoli P, Negrini M, Croce CM (2005) MicroRNA gene expression deregulation in human breast cancer. Cancer Res 65:7065–7070

Jing Q, Huang S, Guth S, Zarubin T, Motoyama A, Chen J, DiPadova F, Lin SC, Gram H, Han J (2005) Involvement of microRNA in AU-rich element-mediated mRNA instability. Cell 120:623–634

Lau NC, Lim LP, Weinstein EG, Bartel DP (2001) An abundant class of tiny RNAs with probable regulatory roles in Caenorhabditis elegans. Science 294:858–862

Lewis BP, Shih IH, Jones-Rhoades MW, Bartel DP, Burge CB (2003) Prediction of mammalian microRNA targets. Cell 115:787–798

Lim LP, Lau NC, Garrett-Engele P, Grimson A, Schelter JM, Castle J, Bartel DP, Linsley PS, Johnson JM (2005) Microarray analysis shows that some microRNAs downregulate large numbers of target mRNAs. Nature 433:769–773

Liu W, Mao SY, Zhu WY (2007) Impact of tiny miRNAs on cancers. World J Gastroenterol 13:497–502

Lozzio CB, Lozzio BB (1973) Cytotoxicity of a factor isolated from human spleen. J Natl Cancer Inst 50:535–538

Mazière P, Enright AJ (2007) Prediction of microRNA targets. Drug Discov Today 12:452–458

Nakabayashi H, Taketa K, Yamane T, Oda M, Sato J (1985) Hormonal control of alpha-fetoprotein secretion in human hepatoma cell lines proliferating in chemically defined medium. Cancer Res 45:6379–6383

Puck TT, Marcus PI, Cieciura SJ (1956) Clonal growth of mammalian cells in vitro; growth characteristics of colonies from single HeLa cells with and without a feeder layer. J Exp Med 103:273–283

Rasheed S, Nelson-Rees WA, Toth EM, Arnstein P, Gardner MB (1974) Characterization of a newly derived human sarcoma cell line (HT-1080). Cancer 33:1027–1033

Rehwinkel J, Natalin P, Stark A, Brennecke J, Cohen SM, Izaurralde E (2006) Genome-wide analysis of mRNAs regulated by Drosha and Argonaute proteins in Drosophila melanogaster. Mol Cell Biol 26:2965–2975

van Rooij E, Sutherland LB, Liu N, Williams AH, McAnally J, Gerard RD, Richardson JA, Olson EN (2006) A signature pattern of stress-responsive microRNAs that can evoke cardiac hypertrophy and heart failure. Proc Natl Acad Sci USA 103:18255–18260

Scherer WF, Syverton JT, Gey GO (1953) Studies on the propagation in vitro of poliomyelitis viruses. IV. Viral multiplication in a stable strain of human malignant epithelial cells (strain HeLa) derived from an epidermoid carcinoma of the cervix. J Exp Med 97:695–710

Schneider U, Schwenk HU, Bornkamm G (1977) Characterization of EBV-genome negative "null" and "T" cell lines derived from children with acute lymphoblastic leukemia and leukemic transformed non-Hodgkin lymphoma. Int J Cancer 19:621–626

Sempere LF, Freemantle S, Pitha-Rowe I, Moss E, Dmitrovsky E, Ambros V (2004) Expression profiling of mammalian microRNAs uncovers a subset of brain-expressed microRNAs with possible roles in murine and human neuronal differentiation. Genome Biol 5:R13

Sevignani C, Calin GA, Siracusa LD, Croce CM (2006) Mammalian microRNAs: a small world for fine-tuning gene expression. Mamm Genome 17:189–202

Sood P, Krek A, Zavolan M, Macino G, Rajewsky N (2006) Cell-type-specific signatures of microRNAs on target mRNA expression. Proc Natl Acad Sci USA 103:2746–2751

Soule HD, Vazguez J, Long A, Albert S, Brennan M (1973) A human cell line from a pleural effusion derived from a breast carcinoma. J Natl Cancer Inst 51:1409–1416

Suh MR, Lee Y, Kim JY, Kim SK, Moon SH, Lee JY, Cha KY, Chung HM, Yoon HS, Moon SY, Kim VN, Kim KS (2004) Human embryonic stem cells express a unique set of microRNAs. Dev Biol 270:488–498

Suzuki R, Shimodaira H (2006) Pvclust: an R package for assessing the uncertainty in hierarchical clustering. Bioinformatics 22:1540–1542

Takamizawa J, Konishi H, Yanagisawa K, Tomida S, Osada H, Endoh H, Harano T, Yatabe Y, Nagino M, Nimura Y, Mitsudomi T, Takahashi T (2004) Reduced expression of the let-7 microRNAs in human lung cancers in association with shortened postoperative survival. Cancer Res 64:3753–3756

Tsuchiya S, Okuno Y, Tsujimoto G (2006) MicroRNA: biogenetic and functional mechanisms and involvements in cell differentiation and cancer. J Pharmacol Sci 101:267–270

Zeng Y (2006) Principles of micro-RNA production and maturation. Oncogene 25:6156–6162

Secreted CXCL1 Is a Potential Mediator and Marker of the Tumor Invasion of Bladder Cancer

Hiroaki Kawanishi,[1] Yoshiyuki Matsui,[1] Masaaki Ito,[1] Jun Watanabe,[1] Takeshi Takahashi,[1] Koji Nishizawa,[1] Hiroyuki Nishiyama,[1] Toshiyuki Kamoto,[1] Yoshiki Mikami,[2] Yoshinori Tanaka,[4] Giman Jung,[4] Hideo Akiyama,[4] Hitoshi Nobumasa,[4] Parry Guilford,[5,6] Anthony Reeve,[5] Yasushi Okuno,[3] Gozoh Tsujimoto,[3] Eijiro Nakamura,[1] and Osamu Ogawa[1]

Abstract

Purpose: The purpose of this study was to identify proteins that are potentially involved in the tumor invasion of bladder cancer.

Experimental Design: We searched for the candidate proteins by comparing the profiles of secreted proteins among the poorly invasive human bladder carcinoma cell line RT112 and the highly invasive cell line T24. The proteins isolated from cell culture supernatants were identified by shotgun proteomics. We found that CXCL1 is related to the tumor invasion of bladder cancer cells. We also evaluated whether the amount of the chemokine CXCL1 in the urine would be a potential marker for predicting the existence of invasive bladder tumors.

Results: Higher amount of CXCL1 was secreted from highly invasive bladder carcinoma cell lines and this chemokine modulated the invasive ability of those cells *in vitro*. It was revealed that CXCL1 regulated the expression of matrix metalloproteinase-13 *in vitro* and higher expression of CXCL1 was associated with higher pathologic stages in bladder cancer *in vivo*. We also showed that urinary CXCL1 levels were significantly higher in patients with invasive bladder cancer (pT1-4) than those with noninvasive pTa tumors ($P = 0.0028$) and normal control ($P < 0.0001$). Finally, it was shown that CXCL1 was an independent factor for predicting the bladder cancer with invasive phenotype.

Conclusions: Our results suggest that CXCL1 modulates the invasive abilities of bladder cancer cells and this chemokine may be a potential candidate of urinary biomarker for invasive bladder cancer and a possible therapeutic target for preventing tumor invasion.

Bladder cancer is the fourth most common cancer in the United States and it will be responsible for the death of an estimated 13,060 persons in the United States alone during 2006 (1, 2). Bladder cancer is generally classified into superficial (non-muscle invasive) or muscle-invasive cancer based on the natural history of these tumors. Most bladder cancers (~80%) present as superficial tumors, which include Ta (noninvasive) or T1 (lamina propria invasive) tumor. Among these superficial tumors, ~70% recur after transurethral resection and 10% to 20% show progression to become muscle-invasive (T2-4) tumors. T1 tumors are more likely to progress to muscle-invasive disease (25-40%) than Ta tumors (3-4%; ref. 3). Muscle-invasive cancer has a much less favorable prognosis than superficial cancer (4). Due to the unfavorable prognosis of muscle-invasive cancer, there is considerable interest in developing markers that can identify superficial cancers with a high risk of progression. The identification of this type of marker will contribute to the early detection of life-threatening invasive bladder cancer and the improvement of the prognosis of this disease.

Multifocality and frequent recurrence is also another characteristic of bladder cancers (5). Multifocal tumors often present with varying degrees of stage and grade. Most studies have found only monoclonal tumors. The presence of shared genetic changes in all tumors resected from individual patients suggests that these are related lesions that have evolved from a single altered cell clone. However, there are some examples of more than one unrelated monoclonal tumor in the same bladder (oligoclonality), and this is not surprising given the association of transitional cell carcinoma risk with smoking and the pan-urothelial carcinogenic insult associated with this (6). There are two types of bladder cancer with fundamentally

Authors' Affiliations: Departments of [1]Urology and [2]Pathology, Graduate School of Medicine and [3]Department of Genomic Drug Discovery Science, Graduate School of Pharmaceutical Sciences, Kyoto University, Kyoto, Japan; [4]New Frontiers Research Laboratories, Toray Industries, Inc., Kanagawa, Japan; and [5]Cancer Genetics Laboratory, University of Otago; [6]Pacific Edge Biotechnology Ltd., Dunedin, New Zealand

Received 8/5/07; revised 12/29/07; accepted 1/17/08.

Grant support: Grant-in-Aid from the Ministry of Education, Culture, Sports, Science and Technology of Japan, Kurozumi Medical Foundation, and Takeda Science Foundation (E. Nakamura) and The New Energy and Industrial Technology Development Organization of Japan (O. Ogawa).

The costs of publication of this article were defrayed in part by the payment of page charges. This article must therefore be hereby marked *advertisement* in accordance with 18 U.S.C. Section 1734 solely to indicate this fact.

Note: Supplementary data for this article are available at Clinical Cancer Research Online (http://clincancerres.aacrjournals.org/).

Requests for reprints: Eijiro Nakamura, Department of Urology, Kyoto University Graduate School of Medicine, 54 Shogoinkawahara-cho, Sakyo-ku, 606-8507 Kyoto, Japan. Phone: 81-75-751-3325; Fax: 81-75-761-3441; E-mail: hap@kuhp.kyoto-u.ac.jp.

doi:10.1158/1078-0432.CCR-07-1922

different genetic alterations and clinical outcome. Whereas noninvasive tumors are genetically stable and characterized by frequent FGFR3 mutations and deletions of chromosome 9q, invasive bladder cancer are characterized by gross chromosomal instability and many genetic alterations. Alterations in both p53 and Rb tumor gene suppressor pathways are well documented in invasive bladder cancer. Additionally, numerous markers, such as cell adhesion molecules, tumor-associated antigens, proliferating antigens, and cell cycle regulatory proteins, have been identified, which correlate to some extent with tumor stage and prognosis (7). However, the power of many of these biomarkers in detecting superficial disease or predicting the clinical outcome of individual tumors is limited, and alternative markers are still in demand.

Secreted proteins determine, control, and coordinate many of the biological processes in organisms, such as cellular growth, differentiation, and tumorigenesis (8). After the completion of the Human Genome Project, many researchers have hypothesized that the best cancer biomarkers will probably be secreted proteins (9). Thus, great interest is currently being focused on the characterization of proteins secreted by isolated tumor cells and neoplastic tissues to identify novel biomarkers and new molecular targets for therapy.

Approximately 20% to 25% of all cellular proteins undergo secretion (10); however, the quantity of each protein secreted is usually very low. Analysis of culture supernatants after incubation of cells seems to be a reasonable way to identify such secreted proteins. However, even minor contamination with protein-rich FCS can easily mask secreted proteins of interest. Recently, we established a new method for analyzing the proteins in cell culture supernatants by using serum-free medium. Using this method, we identified clusterin as a marker for the hypoxia-inducible factor–independent function of von Hippel-Lindau protein and revealed its role in the development of familial pheochromocytoma (11, 12). In these studies, secreted proteins in the serum-free medium were precipitated with trichloroacetic acid and analyzed by two-dimensional PAGE. Then, protein spots of interest were identified by mass spectrometry (MS) analysis. Although two-dimensional PAGE provides information about the position of protein spots, it may not be so effective for detecting scarce secreted proteins (13). In the present study, we improved our method by using multidimensional shotgun proteomics, a powerful proteomics analysis tool with a high efficiency to identify hundreds of proteins in a single run (14, 15). Using this method, we compared the proteome of secreted proteins in the culture supernatant from bladder cancer cell lines with different invasive phenotypes and found that CXCL1 is overexpressed in invasive bladder cancer.

Materials and Methods

Cell lines and cell culture. Six human bladder cancer cell lines were used: DSH1 (16), KU-7 (17), RT112 (18), UMUC-3 (19), 5637 (20), and T24 (21). The cell lines were cultured in RPMI 1640 (Sigma Chemical Co.) supplemented with 10% FCS, 12.5 mmol/L HEPES, and penicillin-streptomycin at 37°C in 5% CO_2.

Cell invasion assay. BD Biocoat Matrigel Invasion Chambers (Becton Dickinson) were used. Cells were suspended to a concentration of 1×10^5/mL in serum-free RPMI 1640. The cell suspension (500 μL) was added to the insert of the Matrigel-coated invasion chamber (24 well and 8-μm pore size) and incubated with RPMI 1640 with 10% FCS in the bottom of the chamber at 37°C in 5% CO_2. Incubation time was modified according to the invasive ability of the cell lines. Noninvading cells were removed by wiping with cotton swabs and the cells that attached to the lower surface of the membrane were fixed with 70% ethanol. Cells were then stained with hematoxylin and counted using a microscope (Eclipse E1000M, Nikon). Invading cells were quantified by counting the number of cells in the five densest spots identified on the lower surface of the filter within a single ×200 field. Each experiment was done in triplicate.

Processing of cell culture supernatants. RT112 and T24 were grown to 70% to 80% confluence in RPMI 1640 with 10% FCS in 100-mm dishes. The cells were washed with PBS thrice and cultured in 10 mL serum-free RPMI 1640. In pilot experiments, we found that these cell lines proliferate for at least 2 d when grown in serum-free RPMI 1640 (data not shown). Twenty-four hours later, cell culture supernatants were collected from four dishes (40 mL) and centrifuged at 150,000 × *g* and 4°C for 30 min in a Beckman Optima XL-100 ultracentrifuge (Beckman Coulter) to remove cells and cell debris completely. The supernatants were then concentrated to ~1 mL (0.6 mg/mL) by using an Amicon Ultra centrifugal filter device (15 mL, 5K NMWL; Millipore). Protein in RPMI 1640 with 10% FCS was collected in the same way as the conditioned medium and used as a control. Total protein (120 μg) was fractionized with the ProteomeLab PF 2D Protein Fractionation System (Beckman Coulter). The separation was done using a PF2D HPRP column (Beckman Coulter) at 50°C with a flow rate of 0.75 mL/min. The column was equilibrated with solvent A [0.1% (v/v) trifluoroacetic acid in water] and eluted with solvent B [0.08% (v/v) trifluoroacetic acid in 100% (v/v) acetonitrile]. The gradient was 0% to 100% solvent B for 30 min. Eluent from column was automatically collected every 30 s into the 96-well plate with a fraction collector. Comparing the chromatogram profiles, fractions with peaks originating from FCS were excluded from further analysis. Fractions with specific peaks for cell culture supernatants were pooled into seven fractions, lyophilized, and resuspended in 100 μL of 20 mmol/L ammonium bicarbonate buffer (pH 8.0).

Two-dimensional liquid chromatography-MS/MS and data analysis. After trypsination of the fractions, two-dimensional liquid chromatography-MS/MS shotgun analysis was done by using an online nano-liquid chromatography system (Dina system, KYA Technologies) and a quadrupole time-of-flight mass spectrometer (Q-Tof Premier, Waters Micromass) as previously described (22). The identified proteins were obtained from MS/MS experiments by Mascot software (Matrix Science) using the Swiss-Prot human protein database containing 13,799 entries of human proteins (April 2006). The proteins were considered identified if they had resulting Mascot scores of >35 and at least two peptides with score >20. To determine the cellular localization of identified proteins, we used the information available from Swiss-Prot database.

cDNA microarray. Bladder cancer tissues for cDNA microarray analysis were obtained with informed consent from 55 patients who underwent surgery at our hospital. Tumor staging was assessed according to tumor-node-metastasis classifications (26 pTa, 11 pT1, 3 pT2, 13 pT3, and 2 pT4). Each bladder cancer sample was obtained by cold-cup biopsy at the time of transurethral surgery. As for the substitution of normal urothelium in the bladder, ureteral urothelium was obtained from 16 patients who had undergone nephrectomy for renal cell carcinoma. Ureteral urothelium was removed from the surgical specimen and the adjacent portion of the specimen was examined pathologically to confirm that neither urothelial dysplasia nor malignancy existed. Microarray experiments were done using a cDNA array containing ~30,000 50-mer oligonucleotides (MWG Biotech AG) fabricated by Pacific Edge Biotechnology Ltd. in New Zealand as described (23). In each hybridization, fluorescent cDNA targets were prepared from a tissue RNA sample and a reference RNA sample was derived from a pool of cell lines of different cancers. The

differences of gene expression profiles between T24 cells treated with anti-CXCL1 neutralizing antibodies or control IgG were examined by Human Genome U133 Plus 2.0 Array (Affymetrix, Inc.). cRNA preparation and hybridization to oligonucleotide arrays were according to Affymetrix protocol.

Reverse transcription-PCR. The primer sequences used for reverse transcription-PCR (RT-PCR) were as follows: CXCL1, 5′-CCAGACCCGCCTGCTG-3′ (forward) and 5′-CCTCCTCCCTTCTGGTCAGTT-3′ (reverse); CXCR2, 5′-ATTCTGGGCATCCTTCACAG-3′ (forward) and 5′-TGCACTTAGGCAGGAGGTCT-3′ (reverse); matrix metalloproteinase-13 (MMP-13), 5′-TCTGAACTGGGTCTTCCAAAA-3′ (forward) and 5′-GCATCTACTTTATCACCAATTCCT-3′(reverse); glyceraldehyde-3-phosphate dehydrogenase, 5′-GAAGGTGAAGGTCGGAGTC-3′ (forward) and 5′-GAAGATGGTGATGGGATTTC-3′(reverse). *Glyceraldehyde-3-phosphate dehydrogenase* was used as a housekeeping gene. Real-time quantitative PCR with SYBR Green was done using the GeneAmp 5700 Sequence Detection System (PE Applied Biosystems-Roche). The expression of MMP-13 was quantified relative to glyceraldehyde-3-phosphate dehydrogenase. The thermal profile consisted of 1 cycle at 95°C for 10 min followed by 40 cycles with 15 s at 95°C, 30 s at 60°C, 30 s at 72°C, and 10 s at 78°C. All measurements were done in duplicate.

Detection of CXCL1 proteins. Cells (3.5×10^5) were seeded in 60-mm dishes containing RPMI 1640 with 10% FCS. The medium was removed after 24 h, and the cells were then washed with PBS and further cultured in RPMI 1640 with 10% FCS. After 24 h, CXCL1 protein levels in cell-free culture supernatants were determined using the commercial Quantikine ELISA kit (R&D Systems) according to the manufacturer's instructions. Protein levels were corrected for the total protein in the cell lysate.

Immunohistochemical analysis. Tissues were fixed in 10% buffered formalin and embedded in paraffin. Paraffin blocks were cut at 5 μm thickness. Sections were deparaffinized and rehydrated. For CXCL1 staining, endogenous peroxidase activity was blocked with hydrogen peroxidase. The glass slides were washed in PBS (six times, 5 min each) and mounted with 1% rabbit normal serum in PBS for 30 min. Anti-human CXCL1 polyclonal antibody (1:150; Santa Cruz Biotechnology, Inc.) was used as the primary antibody. The sections were incubated overnight at 4°C, after which Histofine Simple Stain MAX PO (Nichirei Bioscience) was applied, and the subsequent antibody/enzyme conjugate was developed with diaminobenzidine. The sections were lightly counterstained with hematoxylin. MMP-13 staining was done by using an avidin-biotinylated peroxidase complex method (Vectastain Elite ABC kit, Vector Laboratories) as described by Bostrom et al. (24). Anti-human MMP-13 monoclonal antibody was from Daiichi Fine Chemical. A brown precipitate in the cytoplasm indicated a positive immunoreactivity in both proteins. Negative controls consisted of slides where the primary antibody had been omitted. Cases were evaluated as positive staining if >10% of the cytoplasm of the tumor cells was stained. All scoring was conducted in a blind fashion by a trained pathologist (Y.M.).

Knockdown of CXCL1 by RNA interference vector. Small interfering oligonucleotides specific for CXCL1 were designed on the Takara Bio Web site[7] and the oligonucleotide sequences used in the construction of the RNA interference (RNAi) vector were as follows: RNAi 1, 5′-GATCCGCACACTGTCCTATTATATTAGTGCTCCTGGTTGATATAATAGGACAGTGTGCTTTTTTAT-3′ and 5′-CGATAAAAAAGCACACTGTCCTATTATATCAACCAGGAGCACTAATATAATAGGACAGTGTGCG-3′; RNAi 2, 5′-GATCCGCAAATGGCCAATGAGATCATAGTGCTCCTGGTTGTGATCTCATTGGCCATTTGCTTTTTTAT-3′ and 5′-CGATAAAAAAGCAAATGGCCAATGAGATCACAACCAGGAGCACTATGATCTCATTGGCCATTTGCG-3′. The oligonucleotides were annealed and then ligated into *Bam*HI/*Cla*I sites of the pSINsi-hU6 vector (Takara Bio). A retroviral supernatant was obtained by transfection of G3T-hi cells using a Retrovirus Packaging Kit Ampho (Takara Bio). T24 cells were infected with the viral supernatant, and the cells were then selected with 750 μg/mL G418 for 2 to 3 wk. Stable CXCL1 knockdown clones were selected and confirmed by RT-PCR and ELISA.

Establishment of stable transformants of CXCL1. The full-length human CXCL1 cDNA was generated by RT-PCR using Pfu polymerase (Stratagene) from total RNA isolated from T24. The primers used for amplification were the following: 5′-CCAGACCCGCCTGCTG-3′ (forward) and 5′-CCTCCTCCCTTCTGGTCAGTT-3′ (reverse). The PCR product was ligated into *Xho*I/*Bam*HI sites of pcDNA3.1(-) vector (Invitrogen). RT112 cells were transfected with CXCL1 cDNA using Lipofectamine 2000 (Life Technologies, Inc.). Single clones of the stable transfectants were selected with 900 μg/mL G418. Each clone was checked for expression of CXCL1 by RT-PCR and ELISA.

Growth inhibition assay. RT112 and T24 cells (1×10^3 and 4×10^3, respectively) were seeded into 96-well plates in quintuplicate in RPMI 1640 with 10% FCS and allowed to adhere overnight. The cultures were then washed and refed with medium. Cells were incubated for 24 to 48 h. For treatment with neutralizing antibodies, monoclonal anti-CXCL1 or control antibody (mouse IgG; R&D Systems) was added to the medium. Proliferative activity was determined by the 3-(4,5-dimethylthiazol-2-yl)-2,5-diphenyltetrazolium bromide assay using a microtiter plate reader at 540 nm.

Measurement of urinary CXCL1 levels. Clean-catch urine specimens at clinic visits were collected throughout a period of several months from patients seen in our hospital. The control group consisted of outpatients attending with diseases of the urological tracts ($n = 31$, ages 48-84 y; benign prostatic hyperplasia in 14, prostate cancer in 9, lithiasis in 4, neurogenic bladder in 2, renal cancer in 1, and adrenal tumor in 1). Bladder cancer group consists of 67 patients (ages 47-90 y) before undergoing transurethral resection of bladder tumor for later histologically confirmed urothelial cancer (32 pTa, 23 pT1, and 12 pT2-4). There were no age differences between control group and bladder cancer group. These groups do not include the urine samples with >30 leukocytes/microscopic field. Collected samples were centrifuged for 10 min at 2,000 rpm at room temperature to remove debris, aliquoted, and stored -80°C. On the day of analysis, frozen urine samples were thawed quickly, and the urinary CXCL1 levels were measured using the Quantikine ELISA kit. Urine creatinine levels were measured spectrophotometrically using the alkaline picrate method.

Statistical analysis. The raw microarray data were analyzed using the nonparametric Mann-Whitney *U* test to compare the gene expression level between noninvasive pTa tumors and invasive pT1-4 tumors. The results of urinary CXCL1 levels were analyzed using the Mann-Whitney *U* test for two-group comparisons. The optimal sensitivity and specificity of the urinary CXCL1 levels for diagnosis of bladder cancer and for staging were determined by receiver operating characteristic (ROC) curve analysis using R statistical package. Univariable and multivariable logistic regression models were used to calculate odds ratios and 95% confidence intervals. Statistical analysis of the data was done using the StatView-J 5.0 program (Abacus Concepts, Inc.). A value of $P < 0.05$ was considered statistically significant.

Results

Evaluation of in vitro *invasiveness of bladder cancer cell lines and their proteome in cell culture supernatant.* We choose six different bladder cancer cell lines. Of them, three cell lines, DSH1, KU-7, and RT112 cells, are commonly used as models of superficial bladder cancer and UMUC-3, 5637, and T24 cells are generally used as models of invasive bladder cancer. Then, we examined their invasion ability *in vitro* by using a modified Boyden chamber assay. As shown in Fig. 1A, the number of cells infiltrated was higher in the latter group of cells; this result

[7] http://www.takara-bio.co.jp/

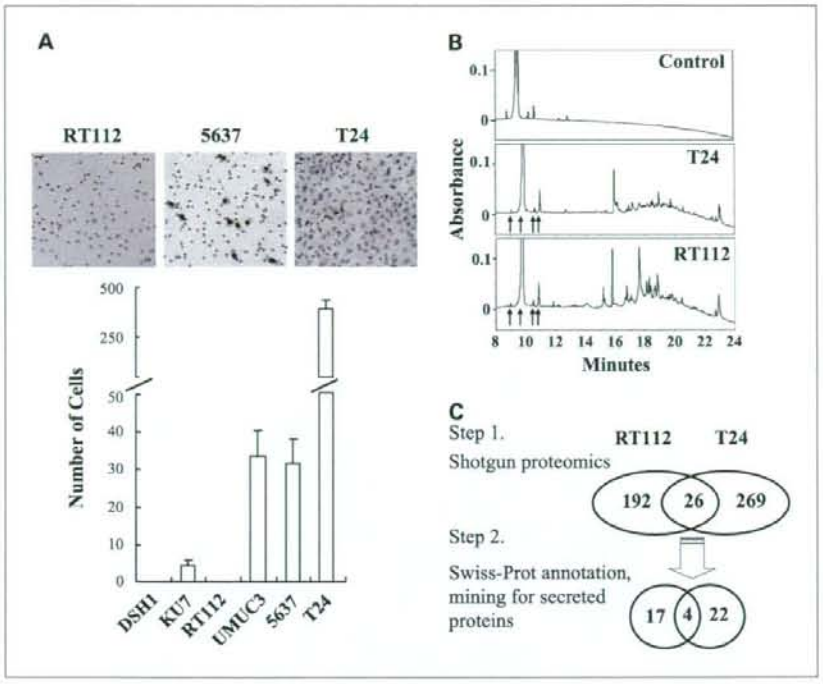

Fig. 1. *A*, invasion of bladder cancer cell lines in a modified Boyden chamber. Cells (5×10^4) were seeded into the upper compartment of the chamber in serum-free RPMI 1640 and incubated for 24 h at 37°C. RPMI 1640 with 10% FCS filled the lower compartment. Columns, mean of the number of cells in the five densest spots identified on the lower surface of the filter within a single ×200 field in each of three experiments; bars, SD. *B*, reverse-phase chromatograms of cell culture supernatants. Eluted proteins were detected by UV absorbance at 214 nm. In T24 and RT112 supernatant, peaks originating from FCS are indicated by arrows. The fractions from 11 to 23 min were collected for two-dimensional liquid chromatography-MS/MS analysis. *C*, schematic flow diagram depicting the steps for identifying proteins associated with invasion by human bladder cancer.

indicated that UMUC-3, 5637, and T24 are highly invasive, whereas DSH1, KU-7, and RT112 are poorly invasive tumor cells. DSH1 and RT112 showed almost no invasion ability and T24 cells exhibited the strongest invasive ability.

Because secreted proteins are thought to be suitable targets for the development of diagnostic markers and/or for identification of new drug targets (8, 9), we attempted to identify secreted proteins that were potentially involved or associated with the invasion of bladder cancer through the proteomic comparison of culture supernatants from highly invasive T24 and less invasive RT112 cells. As protein-rich FCS could easily mask proteins of interest in this analysis, we used serum-free medium as described previously (11, 12) and excluded contamination as far as possible by removing chromatogram fractions with peaks originating from FCS. As shown in Fig. 1B, fractions eluted from 11 to 23 min, which seemed to be produced from cultured cells, were pooled and analyzed by shotgun proteomics. A total of 477 proteins were identified in the culture supernatants of RT112 and T24 cells (218 and 295 proteins, respectively). Swiss-Prot database annotated the cellular localization of 330 proteins and 43 of them were predicted to be secreted proteins (Fig. 1C). Of these secreted proteins, 22 of them were detected only in highly invasive T24 cells (Supplementary Table S1).

***Up-regulation of CXCL1 in invasive bladder tumors* in vitro *and* in vivo.** To further investigate the significance of these proteins in the invasion of bladder cancer, we compared the proteome data with mRNA expression profiles that consisted of 26 noninvasive pTa tumors and 29 invasive pT1-4 tumors *in vivo* (23). Among those 22 proteins specific for highly invasive T24 cells, there were corresponding probe sets for 14 of them on the custom-made chips. Of them, the expression of CXCL1 was significantly higher in invasive tumors than in noninvasive tumors *in vivo* (Fig. 2A). Additionally, the expression of this gene was more abundant in tumor tissues compared with that in normal uroepithelial cells. To confirm these results, the expression of this gene was examined in bladder cancer cell lines by using RT-PCR. It was revealed that all of the three highly invasive cell lines (UMUC-3, 5637, and T24) expressed CXCL1, whereas neither of them was detected in the less invasive DSH1, KU-7, and RT112 cell lines (Fig. 2B).

Because CXC chemokines are known to contribute to several tumor-related processes, such as tumor growth, angiogenesis/angiostasis, local invasion, and metastasis (25), we next examined the significance of CXCL1 in invasion of bladder cancer cell lines *in vitro*. First, we confirmed that all of the invasive cell lines secreted CXCL1 into the supernatants, whereas none of the less invasive cell lines secreted the detectable levels of this chemokine (Fig. 2C). These results indicate that higher secretion of CXCL1 is associated with the higher invasion ability of bladder cancer cells *in vitro*. It was also confirmed that *CXCR2*, the gene for the receptor of CXCL1, was expressed in all of bladder tumor cell lines irrespective of their invasion ability (Fig. 2B). Because CXCL1 was highly expressed at the mRNA level in invasive bladder tumors *in vivo*, we next examined if this chemokine is also up-regulated at the protein level. Representative results of immunohistochemical staining are shown in Fig. 2D. It was revealed that positive staining was observed in none of the normal uroepithelium samples and in 40% of pTa tumors. On the other hand, as many as 75% of pT1-4 tumors stained positive. These observations led us to hypothesize that the expression of CXCL1 was related to tumor invasion of bladder cancer *in vivo*.

Secreted CXCL1 is sufficient for increased invasion by bladder cancer cells. Next, we clarified whether CXCL1 regulated the invasive ability of bladder cancer cells *in vitro*. We first examined the effect of knockdown of CXCL1 in highly invasive T24 cells by using RNAi vectors. We have established two different polyclones in which the expression of CXCL1 is reduced by 30% compared with mock-transfected control cells (Fig. 3A). It was revealed that this inhibition of CXCL1 expression decreased the number of infiltrated cells in the invasion assay to 30% (Fig. 3B). Because the treatment of T24 cells with anti-CXCL1 neutralizing antibodies resulted in comparable reduction in the number of infiltrating cells, these results suggest that secreted CXCL1 regulates the invasive ability of bladder cancer cells via an autocrine loop (Fig. 3C). As CXCL1 has previously been shown to stimulate cell proliferation as an autocrine growth factor in several cancer cell lines (26, 27), we examined the effect of this chemokine on cell proliferation. As shown in Fig. 3D, the knockdown of CXCL1 or its neutralization with specific antibodies showed no direct effect on proliferation of T24 cancer cell lines. These results indicated that secreted CXCL1 in the supernatant promotes the invasion of T24 cells but has little effect on the proliferation of these cells.

To examine if the expression of CXCL1 is sufficient to promote the enhanced invasion of bladder cancer cell lines, less invasive RT112 cells were stably transfected with a plasmid that encoded CXCL1 and two independent monoclones were established. Both monoclones successfully secreted large amounts of CXCL1 and showed higher invasive ability compared with mock-transfected control cells (Fig. 3E). These results indicated that the expression of CXCL1 is sufficient to promote the enhanced invasion of bladder cancer cells *in vitro*. As observed for T24 cells, this effect was suppressed by treatment with anti-CXCL1 neutralizing antibodies and the forced expression of this chemokine had no effect on the proliferation of RT112 cells (data not shown).

***CXCL1 regulated the expression of MMP-13 in bladder cancer cells* in vitro *and the expression of CXCL1 was associated with that of MMP-13* in vivo.** To clarify the mechanisms by which CXCL1 regulates the invasive ability of bladder cancer, we compared the mRNA expression profiles of highly invasive T24 cells treated with or without an anti-CXCL1 neutralizing antibody using the Affymetrix U133 Plus 2.0 Array. Among the 38,500 transcripts analyzed, we identified 62 RNAs whose abundance was decreased (<0.6-fold) by treatment with an anti-CXCL1 neutralizing antibody (Supplementary Table S2). It was revealed that a member of the MMP family, MMP-13, was down-regulated by the inhibition of CXCL1. To confirm this result, we examined the expression of MMP-13 in T24 and RT112 cells in which CXCL1 was engineered to be repressed or overexpressed, respectively. It was revealed that the expression of MMP-13 was regulated by the expression of CXCL1 in both cell lines (Fig. 4A). Because it has been reported that the expression of MMP-13 is associated with the invasion of bladder cancer *in vivo* (24), we next examined if the up-regulation of CXCL1 is associated with the higher expression of MMP-13 in bladder cancer cells *in vivo*. Positive staining of MMP-13 was observed in none of 11 tumors (6 with pTa, 4 with pT1, and 1 with pT3) with negative staining of CXCL1, whereas it was observed in 9 (1 with pT1, 7 with pT3, and 1 with pT4) of 19 (4 with pTa, 5 with pT1, 1 with pT2, 7 with pT3, and 2 with pT4) tumors with positive staining of that chemokine (Fig. 4B). It was revealed that statically significant correlation was observed between the expressions of both proteins ($P = 0.0064$, χ^2 test). These results suggest the possibility that MMP-13 is also regulated by CXCL1 *in vivo*.

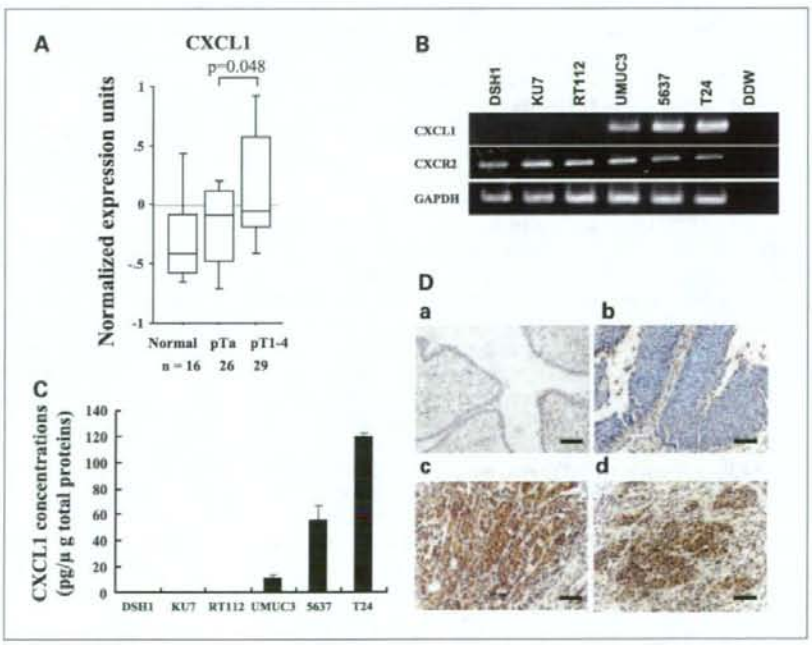

Fig. 2. *A*, cDNA microarray data for CXCL1. The normalized expression units of this gene were transformed into the log2 values. Bars of the box extend from the 25th to 75th percentile of the data and the line in the middle represents the median. The upper and lower bars represent the distance from the 10th to 90th percentile from the median. The Mann-Whitney *U* test was used to compare expression levels between the two groups. *B*, expression of CXCL1 and CXCR2 mRNA by bladder cancer cell lines with different levels of invasiveness. The PCR conditions are as follows: denaturation (95°C, 5 min), 32 cycles of denaturation (94°C, 1 min), annealing (58°C, 1 min), and extension (72°C, 1.5 min). GAPDH, glyceraldehyde-3-phosphate dehydrogenase. Values were corrected for the total protein in the cell lysate. *C*, expression of CXCL1 protein by bladder cancer cell lines. Protein levels in cell culture supernatants were analyzed by ELISA. Each cell line was plated in triplicate; experiments were repeated at least twice. Bars, SD. *D*, immunohistochemical staining for CXCL1 in surgical tissue specimens. A brown precipitate in the cytoplasm denotes positive signal. Representative samples of negative (*a*, normal uroepithelium; *b*, pTaG1) and positive (*c*, pT2G3; *d*, pT3G3) staining are shown. Bars, 100 μm.

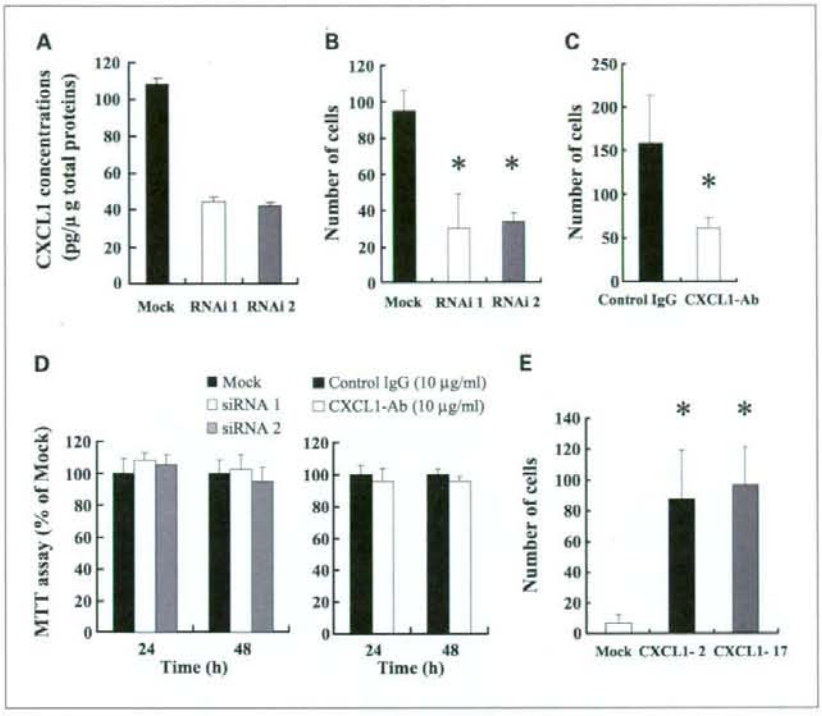

Fig. 3. *A*, knockdown of CXCL1 by RNAi vector in T24 cells was confirmed by ELISA. Values were corrected for the total protein in the cell lysate. Bars, SD. *B*, invasive potential of CXCL1 knockdown clones. After 8 h, the cells on the lower surface of the filter were counted. *, $P < 0.01$, compared with mock clones. *C*, effect of neutralizing antibody to CXCL1 on invasive ability. T24 cells were incubated in RPMI 1640 with 10% FCS containing 10 μg/mL anti-CXCL1 or control IgG for 48 h. Then, the cells were subsequently placed in the upper compartment of an invasion chamber in serum-free RPMI 1640 containing 10 μg/mL anti-CXCL1 or control IgG and incubated at 37°C under 5% CO_2. After 8 h, the cells on the lower surface of the filter were counted. *, $P < 0.05$, compared with control IgG. *D*, effect of CXCL1 knockdown and neutralizing antibody to CXCL1 on proliferation rate of T24 cells. The cell proliferation was determined by the 3-(4,5-dimethylthiazol-2-yl)-2,5-diphenyltetrazolium bromide (*MTT*) assay. No significant difference was detected. *E*, CXCL1 overexpression increased the invasiveness of RT112 cells. After 60 h of incubation, cells on the lower surface of the filter were counted. *, $P < 0.01$, compared with mock clones. Columns, each result of a modified Boyden chamber assay is expressed as the mean of the number of cells in the five densest spots identified on the lower surface of the filter within a single ×200 field in each of three experiments; bars, SD. A representative experiment is shown.

The level of CXCL1 in the urine reflects the existence of bladder cancer. Because immunohistochemical analysis showed that bladder tumors express CXCL1 *in vivo*, we determined if an increase of CXCL1 in the urine could indicate the existence of bladder cancer, especially that with invasive phenotype. The amount of CXCL1 in the urine was examined in 67 patients with histopathologically proven bladder cancer and 31 controls. Because it was shown that several chemokines are elevated in patients with febrile urinary tract infections (28), we eliminated urine samples contaminated with >30 leukocytes per microscopic field. The concentration of CXCL1 in the urine was examined by ELISA and corrected by the urinary creatinine level (Fig. 5A). The mean corrected CXCL1 level in the control group and in patients with noninvasive and invasive tumors was 7.8 ± 2.5, 17 ± 3.7, and 112 ± 25 pg/mg creatinine (mean ± SE), respectively. It was revealed that the corrected CXCL1 level from both noninvasive pTa tumors and invasive pT1-4 tumors was significantly higher than those in the controls ($P = 0.0076$ and $P < 0.0001$, respectively). More importantly, a significant difference was observed between noninvasive and invasive tumors ($P = 0.0028$). These results suggested that the corrected CXCL1 level in the urine would predict the existence of both noninvasive and invasive bladder tumors. So, we have done the ROC curve analysis to estimate the optimal cutoff point. Using 9.5 pg/mg creatinine as the cutoff value to predict the existence of noninvasive or invasive bladder cancer, measurement of the corrected urine CXCL1 level had a sensitivity of 70.1% and a specificity of 80.6% (area under the curve, 0.782; Fig. 5B). Furthermore, using 37.5 pg/mg creatinine as the cutoff value to predict particularly invasive bladder cancer, measurement of corrected CXCL1 had a sensitivity of 57.1% and a specificity of 90.6% (area under the curve, 0.713; Fig. 5C). Finally, we have done multivariate stepwise logistic regression analysis incorporating CXCL1 as a continuous variable, cytology, age, and sex to examine that the corrected CXCL1 level could be an independent factor for predicting the invasive bladder cancer. It was revealed that cytology (odds ratio, 21.82; 95% confidence interval, 3.981-113.780; $P = 0.003$) and CXCL1 (odds ratio, 1.023; 95% confidence interval, 1.001-1.044; $P = 0.038$) were independent factors for predicting the bladder cancer with invasive phenotype (Table 1).

Discussion

Tumor cells overexpress many secreted proteins; some of these can be detected in serum samples from patients with cancer and have been considered as potential new tumor markers (29). Well-known secreted proteins that are used as biomarkers include α-fetoprotein for liver cancer or non-seminomatous germ cell tumors, as well as prostate-specific antigen for prostate cancer (30). Our previous analysis of serum-free cell culture supernatants showed that proteins in the culture supernatant reflected those produced by tumor cells *in vivo* (11). This observation strongly suggests that systematic analysis of the proteins secreted by cultured cancer cells will contribute to the identification of potential diagnostic and prognostic tumor biomarkers.

We compared the protein profile between highly invasive (T24) and less invasive (RT112) bladder cancer cell lines.

Candidate proteins were further screened using the cellular localization information from the Swiss-Prot database. Consequently, CXCL1 was significantly higher in invasive tumors than in noninvasive tumors *in vivo* (Fig. 2A).

CXCL1 is a member of the CXC chemokine family (31). This family of molecules can be classified according to the presence or absence of three amino acid residues (Glu-Leu-Arg; ELR motif) that precede the first cysteine amino acid residue in the primary structure (32). The ELR$^+$ CXC chemokines (CXCL1, CXCL2, CXCL3, CXCL5, CXCL6, CXCL7, and CXCL8) are chemoattractants for neutrophils and are also potent angiogenic factors (33–35). In contrast, ELR$^-$ CXC chemokines (CXCL4, CXCL9, and CXCL10) are chemoattractants for mononuclear cells and are potent inhibitors of angiogenesis (35, 36). In a variety of human cancers, the ELR$^+$ CXC chemokines have been found to be associated with tumorigenesis, angiogenesis, and metastasis (25, 37). The biological functions of ELR$^+$ CXC chemokines are primarily mediated via CXCR2, a seven-transmembrane G protein–coupled receptor. CXCL1 protein was originally purified from the culture supernatant of Hs29T melanoma cells and is also known as melanoma growth stimulatory activity α or growth-related protein α (38, 39). Although the elevated expression of CXCL1 has been reported in a series of human tumors (40, 41), the role of this chemokine in bladder cancer is poorly understood. In this study, we showed that higher expression of CXCL1 was associated with the invasive phenotype of bladder cancer both *in vitro* and *in vivo* (Fig. 2). We also showed that the secreted CXCL1 was sufficient for the invasion of bladder tumors *in vitro* (Fig. 3). Because the CXCL1 receptor CXCR2 is expressed in all the bladder cancer cell lines (Fig. 2B) and in most of the tumor tissues examined irrespective of the invasion phenotype (microarray analysis; data not shown), it is probable that secreted CXCL1 is associated with the invasion of the bladder cancer via an autocrine loop involving its receptor.

CXCL1 did not induce bladder cancer cell proliferation, although it has been shown to promote cell proliferation in several types of tumors. Its interaction with CXCR2 is shown to induce extracellular signal-regulated kinase 1/2 phosphorylation, which then leads to induction of EGR1, and these are responsible for increased cell proliferation (37). Therefore, we examined the extracellular signal-regulated kinase 1/2 pathway in T24 and RT112 cells in which CXCL1 was engineered to be repressed or overexpressed, respectively. It was revealed that CXCL1 did not induce this pathway in bladder cancer cells (data not shown).

As for the mechanisms by which CXCL1 regulates the invasive ability of bladder cancer cells, we found for the first time that this chemokine induced MMP-13 *in vitro* (Fig. 4A). Although it is still uncertain if this is also true *in vivo*, a recent study showed that MMP-13 is highly expressed in invasive bladder tumor tissue (24), supporting our preliminary immunostaining results (Fig. 4B). As for other MMPs, Zhou et al. (42) reported that a glioma cell line overexpressing CXCL1 showed an increase in motility and invasiveness and that CXCL1-transfected cells showed increased expression of MMP-2. However, the expression of MMP-2 was not affected by the introduction of CXCL1 in RT112 cell lines (data not shown). CXCL1 may regulate the invasion of tumors through several types of MMPs. It has also been reported that this chemokine regulates the expression of several proteins, such as β_1 integrin, SPARC (42), vascular endothelial growth factor, and angiopoietin-2 (43). So, several factors including MMP-13 are likely to be involved in CXCL1-mediated regulation of bladder cancer invasion.

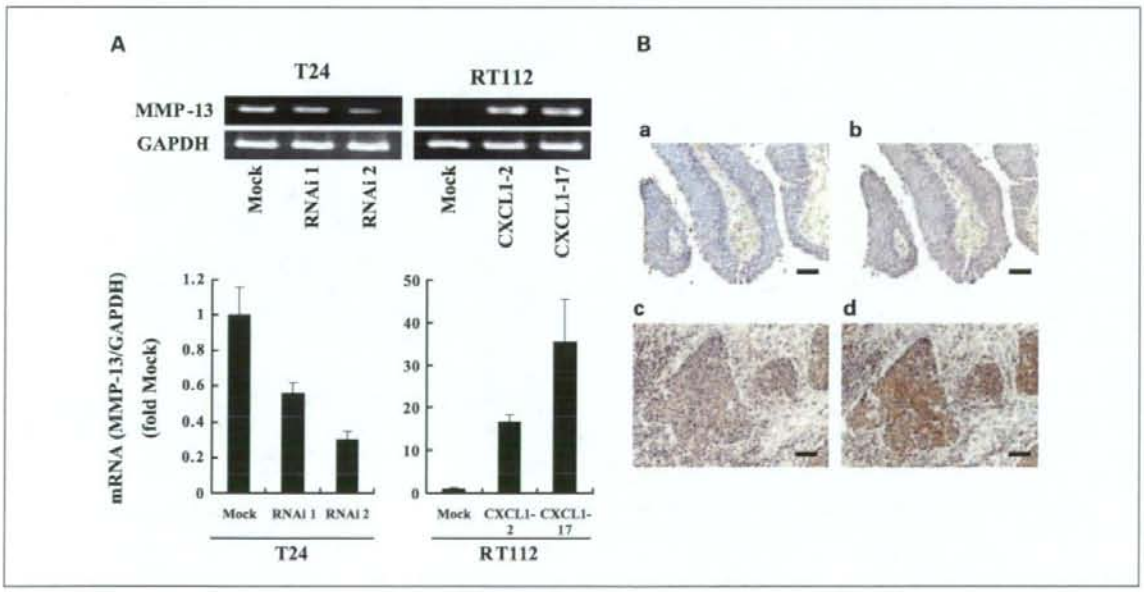

Fig. 4. *A*, expression of MMP-13 mRNA in T24 and RT112 cells in which CXCL1 was engineered to be repressed or overexpressed. RNAi knockdown of CXCL1 in T24 cells resulted in a decreased expression of MMP-13 and RT112 cells engineered to produce CXCL1 acquired the highly increased expression of MMP-13. Top, RT-PCR; bottom, real-time quantitative PCR. Bars, SD. *B*, immunohistochemical staining for CXCL1 and MMP-13 in bladder cancer tissues. Representative samples are shown. *a* and *c*, CXCL1; *b* and *d*, MMP-13. *a* and *b*, pT3G2 tumors showing diffuse cytoplasmic immunoreactivity; *c* and *d*, pTaG1 tumor without specific immunosignal. Bars, 100 μm.

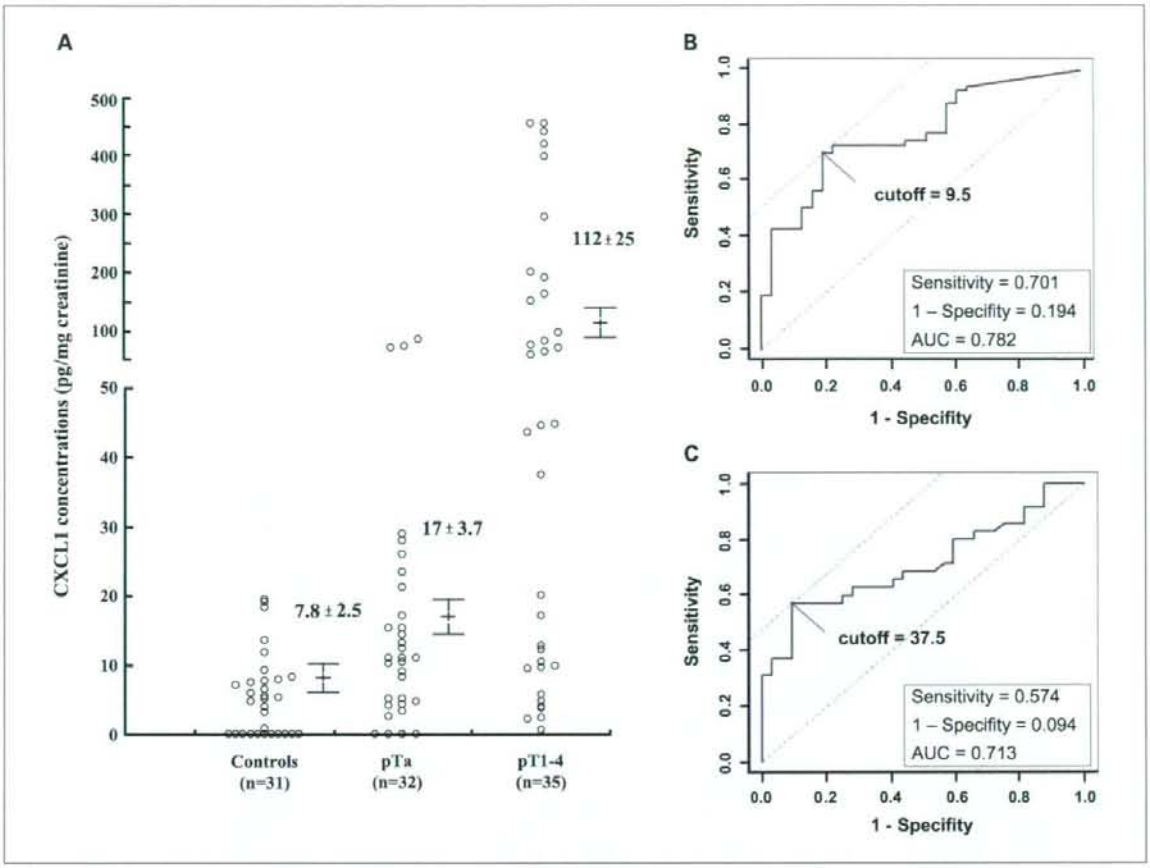

Fig. 5. *A*, CXCL1 levels in the urine of controls and patients with bladder cancer. Values were corrected by the urine creatinine concentration. Points, mean; bars, SE. *B*, ROC curve analysis of the urinary CXCL1 levels. The optimal cutoff of the urinary CXCL1 levels for distinguishing bladder tumor from control was determined as 9.5 using the ROC curve. *C*, ROC curve analysis of the urinary CXCL1 levels for distinguishing invasive from noninvasive bladder tumor. For all patients with bladder tumor, the optimal cutoff value of the urinary CXCL1 levels for distinguishing invasive from noninvasive bladder tumor was determined as 37.5 using ROC curve analysis.

Many studies have focused on the detection of specific bladder cancer–associated proteins in the urine of patients. Thus far, BTA, BTA stat, NMP22, and fibrinogen degradation products have been used as commercial diagnostic markers for bladder cancer in the urine (44). In addition, a lot of soluble urine marker is reported (45, 46). However, none of these markers is sensitive enough for routine clinical use (44). Recently, several investigators have proposed that high-throughput technologies, such as gene expression microarrays or proteomics, may be a new way to identify biomarkers for urothelial cancer in the urine (7, 47), and it is expected that this technology will be more widely used to identify novel cancer biomarkers in the future. In the present study, we showed for the first time that the level of CXCL1 was elevated in the urine from patients with bladder cancer (Fig. 5). These results indicate that an elevated CXCL1 in the urine could predict the existence of bladder cancer, especially in patients with invasive disease. Our results suggest that measurement of the level of CXCL1 in urine may be a useful biomarker for the early detection of invasive bladder cancer, and the inhibition of signals through CXCL1 might be a potent therapeutic target for preventing the progression of the bladder cancer. Additionally, CXCL8, one of ELR CXC chemokines that share 44% amino acid sequence identity with CXCL1 and are reported to be elevated in the urine of patients with transitional cell carcinoma (48). Further prospective and comparative studies in a different population are required for the precise evaluation of diagnostic values of CXC chemokines in bladder cancer.

Table 1. Multivariable stepwise logistic regression analyses of CXCL1, cytology, age, and sex for prediction of invasive stage (≥T1)

Variable	Odds ratio (95% confidence interval)	*P*
CXCL1*	1.023 (1.001-1.044)	0.038
Cytology (positive vs negative)	21.82 (3.981-113.7)	0.003

*Urinary CXCL1 levels were analyzed as continuous variables.

The role of chronic inflammation in cancer progression continues to gain importance in the biological events for several types of cancers. Recurrent or persistent inflammation may induce, promote, or influence susceptibility to carcinogenesis by causing DNA damage, inciting tissue reparative proliferation, and/or creating a stromal "soil" that is enriched with cytokines and growth factors (49). The evidence for an association between chronic inflammation and squamous cell carcinoma of the bladder is strong and widely accepted. In transitional cell carcinoma of the bladder, several animal and human studies strongly support the hypothesis that chronic inflammation induced by persistent urinary tract infections plays a role in the bladder carcinogenesis (50). As CXC chemokines, including CXCL1, play major roles in inflammation and wound healing (25). So, further understanding of roles of these chemokines on the tumorigenesis and disease progression of bladder cancer will be required to provide a new rationale for targeted therapy for this tumor.

Acknowledgments

We thank all members of Urine test room, Department of Clinical Laboratory, Kyoto University Hospital, for analyzing urine samples and Tomoko Matsushita and Chie Hagihara for their valuable technical assistance.

References

1. Borden LS, Jr., Clark PE, Hall MC. Bladder cancer. Curr Opin Oncol 2003;15:227–33.
2. Jemal A, Siegel R, Ward E, et al. Cancer statistics, 2006. CA Cancer J Clin 2006;56:106–30.
3. Lapham RL, Ro JY, Staerkel GA, Ayala AG. Pathology of transitional cell carcinoma of the bladder and its clinical implications. Semin Surg Oncol 1997;13:307–18.
4. Juffs HG, Moore MJ, Tannock IF. The role of systemic chemotherapy in the management of muscle-invasive bladder cancer. Lancet Oncol 2002;3:738–47.
5. Knowles MA. Molecular subtypes of bladder cancer: Jekyll and Hyde or chalk and cheese? Carcinogenesis 2006;27:361–73.
6. Hafner C, Knuechel R, Zanardo L, et al. Evidence for oligoclonality and tumor spread by intraluminal seeding in multifocal urothelial carcinomas of the upper and lower urinary tract. Oncogene 2001;20:4910–5.
7. Sanchez-Carbayo M. Use of high-throughput DNA microarrays to identify biomarkers for bladder cancer. Clin Chem 2003;49:23–31.
8. Zwickl H, Traxler E, Staettner S, et al. A novel technique to specifically analyze the secretome of cells and tissues. Electrophoresis 2005;26:2779–85.
9. Welsh JB, Sapinoso LM, Kern SG, et al. Large-scale delineation of secreted protein biomarkers overexpressed in cancer tissue and serum. Proc Natl Acad Sci U S A 2003;100:3410–5.
10. Diamandis EP. How are we going to discover new cancer biomarkers? A proteomic approach for bladder cancer. Clin Chem 2004;50:793–5.
11. Nakamura E, Abreu-e-Lima P, Awakura Y, et al. Clusterin is a secreted marker for a hypoxia-inducible factor-independent function of the von Hippel-Lindau tumor suppressor protein. Am J Pathol 2006;168:574–84.
12. Lee S, Nakamura E, Yang H, et al. Neuronal apoptosis linked to EglN3 prolyl hydroxylase and familial pheochromocytoma genes: developmental culling and cancer. Cancer Cell 2005;8:155–67.
13. Rabilloud T. Two-dimensional gel electrophoresis in proteomics: old, old fashioned, but it still climbs up the mountains. Proteomics 2002;2:3–10.
14. He P, He HZ, Dai J, et al. The human plasma proteome: analysis of Chinese serum using shotgun strategy. Proteomics 2005;5:3442–53.
15. Wolters DA, Washburn MP, Yates JR III. An automated multidimensional protein identification technology for shotgun proteomics. Anal Chem 2001;73:5683–90.
16. Williams SV, Sibley KD, Davies AM, et al. Molecular genetic analysis of chromosome 9 candidate tumor-suppressor loci in bladder cancer cell lines. Genes Chromosomes Cancer 2002;34:86–96.
17. Tazaki H, Tachibana M. Studies on KU-1 and KU-7 cells as an *in vitro* model of human transitional cell carcinoma of urinary bladder. Hum Cell 1988;1:78–83.
18. Masters JR, Hepburn PJ, Walker L, et al. Tissue culture model of transitional cell carcinoma: characterization of twenty-two human urothelial cell lines. Cancer Res 1986;46:3630–6.
19. Grossman HB, Wedemeyer G, Ren L, Wilson GN, Cox B. Improved growth of human urothelial carcinoma cell cultures. J Urol 1986;136:953–9.
20. Pfluger KH, Probeck HD, Adler G, Stach-Machado D, Kapmeyer H, Havemann K. Karyotype and ultrastructure of a colony stimulating factor (CSF) producing cell line (5637) originated from a carcinoma of the human urinary bladder. Blut 1986;53:89–100.
21. Williams RD. Human urologic cancer cell lines. Invest Urol 1980;17:359–63.
22. Tanaka Y, Akiyama H, Kuroda T, et al. A novel approach and protocol for discovering extremely low-abundance proteins in serum. Proteomics 2006;6:4845–55.
23. Matsui S, Ito M, Nishiyama H, et al. Genomic characterization of multiple clinical phenotypes of cancer using multivariate linear regression models. Bioinformatics 2007;23:732–8.
24. Bostrom PJ, Ravanti L, Reunanen N, et al. Expression of collagenase-3 (matrix metalloproteinase-13) in transitional-cell carcinoma of the urinary bladder. Int J Cancer 2000;88:417–23.
25. Tanaka T, Bai Z, Srinoulprasert Y, Yang BG, Hayasaka H, Miyasaka M. Chemokines in tumor progression and metastasis. Cancer Sci 2005;96:317–22.
26. Li A, Varney ML, Singh RK. Constitutive expression of growth regulated oncogene (gro) in human colon carcinoma cells with different metastatic potential and its role in regulating their metastatic phenotype. Clin Exp Metastasis 2004;21:571–9.
27. Takamori H, Oades ZG, Hoch OC, Burger M, Schraufstatter IU. Autocrine growth effect of IL-8 and GROα on a human pancreatic cancer cell line, Capan-1. Pancreas 2000;21:52–6.
28. Otto G, Burdick M, Strieter R, Godaly G. Chemokine response to febrile urinary tract infection. Kidney Int 2005;68:62–70.
29. Wu CC, Chien KY, Tsang NM, et al. Cancer cell-secreted proteomes as a basis for searching potential tumor markers: nasopharyngeal carcinoma as a model. Proteomics 2005;5:3173–82.
30. Balk SP, Ko YJ, Bubley GJ. Biology of prostate-specific antigen. J Clin Oncol 2003;21:383–91.
31. Wang D, Yang W, Du J, et al. MGSA/GRO-mediated melanocyte transformation involves induction of Ras expression. Oncogene 2000;19:4647–59.
32. Addison CL, Daniel TO, Burdick MD, et al. The CXC chemokine receptor 2, CXCR2, is the putative receptor for ELR$^+$ CXC chemokine-induced angiogenic activity. J Immunol 2000;165:5269–77.
33. Clark-Lewis I, Dewald B, Geiser T, Moser B, Baggiolini M. Platelet factor 4 binds to interleukin 8 receptors and activates neutrophils when its N terminus is modified with Glu-Leu-Arg. Proc Natl Acad Sci U S A 1993;90:3574–7.
34. Hebert CA, Vitangcol RV, Baker JB. Scanning mutagenesis of interleukin-8 identifies a cluster of residues required for receptor binding. J Biol Chem 1991;266:18989–94.
35. Strieter RM, Polverini PJ, Kunkel SL, et al. The functional role of the ELR motif in CXC chemokine-mediated angiogenesis. J Biol Chem 1995;270:27348–57.
36. Luster AD, Greenberg SM, Leder P. The IP-10 chemokine binds to a specific cell surface heparan sulfate site shared with platelet factor 4 and inhibits endothelial cell proliferation. J Exp Med 1995;182:219–31.
37. Wang B, Hendricks DT, Wamunyokoli F, Parker MI. A growth-related oncogene/CXC chemokine receptor 2 autocrine loop contributes to cellular proliferation in esophageal cancer. Cancer Res 2006;66:3071–7.
38. Richmond A, Lawson DH, Nixon DW, Chawla RK. Characterization of autostimulatory and transforming growth factors from human melanoma cells. Cancer Res 1985;45:6390–4.
39. Richmond A, Thomas HG. Purification of melanoma growth stimulatory activity. J Cell Physiol 1986;129:375–84.
40. Luan J, Shattuck-Brandt R, Haghnegahdar H, et al. Mechanism and biological significance of constitutive expression of MGSA/GRO chemokines in malignant melanoma tumor progression. J Leukoc Biol 1997;62:588–97.
41. Moore BB, Arenberg DA, Stoy K, et al. Distinct CXC chemokines mediate tumorigenicity of prostate cancer cells. Am J Pathol 1999;154:1503–12.
42. Zhou Y, Zhang J, Liu Q, et al. The chemokine GRO-α (CXCL1) confers increased tumorigenicity to glioma cells. Carcinogenesis 2005;26:2058–68.
43. Caunt M, Hu L, Tang T, Brooks PC, Ibrahim S, Karpatkin S. Growth-regulated oncogene is pivotal in thrombin-induced angiogenesis. Cancer Res 2006;66:4125–32.
44. Glas AS, Roos D, Deutekom M, Zwinderman AH, Bossuyt PM, Kurth KH. Tumor markers in the diagnosis of primary bladder cancer. A systematic review. J Urol 2003;169:1975–82.
45. Konety BR, Nguyen TS, Brenes G, et al. Clinical usefulness of the novel marker BLCA-4 for the detection of bladder cancer. J Urol 2000;164:634–9.
46. Lokeshwar VB, Obek C, Pham HT, et al. Urinary hyaluronic acid and hyaluronidase: markers for bladder cancer detection and evaluation of grade. J Urol 2000;163:348–56.
47. Kageyama S, Isono T, Iwaki H, et al. Identification by proteomic analysis of calreticulin as a marker for bladder cancer and evaluation of the diagnostic accuracy of its detection in urine. Clin Chem 2004;50:857–66.
48. Sheryka E, Wheeler MA, Hausladen DA, Weiss RM. Urinary interleukin-8 levels are elevated in subjects with transitional cell carcinoma. Urology 2003;62:162–6.
49. Schottenfeld D, Beebe-Dimmer J. Chronic inflammation: a common and important factor in the pathogenesis of neoplasia. CA Cancer J Clin 2006;56:69–83.
50. Michaud DS. Chronic inflammation and bladder cancer. Urol Oncol 2007;25:260–8.

FEBS Letters 582 (2008) 1444–1450

Establishment of the culture model system that reflects the process of terminal differentiation of connective tissue-type mast cells

Hirotsugu Takano[a], Shunsuke Nakazawa[a], Yasushi Okuno[b], Naritoshi Shirata[a], Sohken Tsuchiya[b], Takayuki Kainoh[a], Seigoh Takamatsu[a], Kazuyuki Furuta[a], Yoshitaka Taketomi[c], Yuko Naito[d], Hiromu Takematsu[d], Yasunori Kozutsumi[d], Gozoh Tsujimoto[b], Makoto Murakami[c,e], Ichiro Kudo[c], Atsushi Ichikawa[f], Kazuhisa Nakayama[a], Yukihiko Sugimoto[a], Satoshi Tanaka[f,g,*]

[a] *Department of Physiological Chemistry, Graduate School of Pharmaceutical Sciences, Kyoto University, Sakyo-ku, Kyoto 606-8501, Japan*
[b] *Department of Genomic Drug Discovery Science, Graduate School of Pharmaceutical Sciences, Kyoto University, Sakyo-ku, Kyoto 606-8501, Japan*
[c] *Department of Health Chemistry, School of Pharmaceutical Sciences, Showa University, 1-5-8 Hatanodai, Shinagawa-ku, Tokyo 142-8555, Japan*
[d] *Laboratory of Membrane Biochemistry and Biophysics, Graduate School of Biostudies, Kyoto University, Sakyo-ku, Kyoto 606-8501, Japan*
[e] *Tokyo Metropolitan Institute of Medical Science, 3-18-22 Honkomagome, Bunkyo-ku, Tokyo 113-8613, Japan*
[f] *Institute for Biosciences, Mukogawa Women's University, Koshien, Nishinomiya, Hyogo 663-8179, Japan*
[g] *Department of Immunobiology, School of Pharmacy and Pharmaceutical Sciences, Mukogawa Women's University, 11-68 Kyuban-cho, Koshien, Nishinomiya, Hyogo 663-8179, Japan*

Received 16 January 2008; revised 11 March 2008; accepted 20 March 2008

Available online 31 March 2008

Edited by Beat Imhof

Abstract To understand physiological roles of tissue mast cells, we established a culture system where bone marrow-derived immature mast cells differentiate into the connective tissue-type mast cell (CTMC)-like cells through modifying the previous co-culture system with Swiss 3T3 fibroblasts. Our system was found to reproducibly mimic the differentiation of CTMCs on the basis of several criteria, such as granule maturation and sensitivity to cationic secretagogues. The gene expression profile obtained by the microarray analyses was found to reflect many aspects of the differentiation. Our system is thus helpful to gain deeper insights into terminal differentiation of CTMCs.

Keywords: Mast cell; Gene expression; Differentiation; G_i

1. Introduction

Mast cells play critical roles not only in anaphylactic responses but also in modulation of diverse innate and acquired immune responses [1,2]. Mast cells originate from hematopoietic progenitor cells and undergo terminal differentiation in tissues where they are resident [3]. It is of great interest to investigate the terminal differentiation process of mast cells in each tissue, since modulation of local immune responses by mast cells should be influenced by their heterogeneity. However, little information is currently available about the heterogeneity and local maturation of tissue mast cells.

Rodent mast cells are generally classified into two populations: connective tissue mast cells (CTMCs) and mucosal mast cells (MMCs) [3,4]. CTMCs are represented by cutaneous and peritoneal mast cells and are characterized by abundant cellular histamine and heparin contents and degranulation in response to cationic secretagogues. Since recent studies demonstrated that CTMCs are involved in a wide variety of immune responses, such as autoimmunity [5], contact hypersensitivity [6], and immune tolerance [7], in addition to anaphylactic responses, detailed analysis and characterization of CTMCs are required. To establish experimental models for CTMCs, an array of attempts has been made using various sources, such as IL-3-dependent bone marrow-derived mast cells (BMMCs) [8,9] and fetal skin cells [10]. However, it remains to be clarified how immature mast cell precursors are differentiated into CTMCs and what kinds of genes regulate this process. To address these questions, we established suitable culture system to develop CTMC-like mast cells by modifying the previous methods, and thereby performed microarray analysis of the gene expression profile during the in vitro terminal differentiation of mast cells.

2. Materials and methods

2.1. Preparation of BMMCs

Specific-pathogen-free, 8–12 week-old female Balb/c mice were obtained from Japan SLC (Hamamatsu, Japan). All animal experiments were performed according to the Guidelines for Animal Experiments of Kyoto University and Mukogawa Women's University. BMMCs were prepared as described previously [11], using 10 ng/ml IL-3 (R&D Systems, Minneapolis, MN) in place of WEHI-3 conditioned medium.

2.2. Co-culture of BMMCs with fibroblasts

The co-culture system was established by modifying the previous method [12]. Swiss 3T3 fibroblasts were seeded with 50% confluency in the same RPMI-1640 medium as BMMCs, treated with 3 μg/ml mitomycin C (Sigma, St. Louis, MO) for 3 h, and further incubated for 3 h in the fresh medium without mitomycin C. BMMCs

*Corresponding author. Address: Department of Immunobiology, School of Pharmacy and Pharmaceutical Sciences, Mukogawa Women's University, 11-68 Kyuban-cho, Koshien, Nishinomiya, Hyogo 663-8179, Japan. Fax: +81 798 41 2792.
E-mail address: s_tanaka@mukogawa-u.ac.jp (S. Tanaka).

Abbreviations: BMMC; bone marrow-derived mast cell; CTMC; connective tissue mast cell; MMC; mucosal mast cell

0014-5793/$34.00 © 2008 Published by Elsevier B.V. on behalf of the Federation of European Biochemical Societies.
doi:10.1016/j.febslet.2008.03.033

(5×10^5 cells/ml) were seeded onto this Swiss 3T3 feeder cells and culture for 4 days in the presence of 100 ng/ml stem cell factor (SCF), which was supplied as the conditioned medium of Sf9 cells infected with the recombinant baculovirus encoding murine SCF [12]. An equal volume of the fresh medium containing 100 ng/ml SCF was added at Day-2. When the feeder cells were replaced at Day-4, whole culture was trypsinized and the contaminating fibroblasts were removed as the adhered cells through repeated plating.

2.3. Protease assay

Mast cells were washed with PBS, lysed in PBS containing 2 M NaCl and 0.5% Triton X-100, and incubated for 30 min on ice. The lysate was centrifuged at $10000 \times g$ for 30 min at 4 °C. Activities of three different types of granule proteases in the resultant supernatants were measured using their specific chromogenic peptide substrates, such as S-2586 (tryptic), S-2288 (chymotryptic), and M-2245 (carboxypeptidase A) [13].

2.4. Degranulation

Mast cells were washed with PIPES buffer (25 mM PIPES–NaOH, pH 7.4, containing 125 mM NaCl, 2.7 mM KCl, 5.6 mM glucose, 1 mM $CaCl_2$, and 0.1% bovine serum albumin) and incubated with the buffer containing compound 48/80 (10 μg/ml, Sigma), substance P (100 μM, Sigma), or A23187 (1 μM, Calbiochem, Darmstadt, Germany) for 30 min. In case of antigen stimulation, mast cells sensitized with 1 μg/ml an anti-DNP IgE (SPE-7, Sigma) for 6 h were stimulated with 30 ng/ml DNP-human serum albumin (Sigma). Degranulation was evaluated by measuring β-hexosaminidase activity.

2.5. Oligonucleotide microarray

Total cellular RNAs were isolated from mast cells using an RNeasy mini kit (QIAGEN, Valencia, CA) according to the manufacturer's instructions. Target RNAs were prepared following technical recommendations found in the Affymetrix Gene Chip Expression Analysis Technical Manual (Affymetrix, Santa Clara, CA). The obtained RNAs were labeled and hybridized to the 430A murine GeneChip (Affymetrix), which contains the oligonucleotide probe set for approximately 22000 genes. We used the RMA (robust multi-array analysis) [14] expression measure that represents the log transform of (background corrected and normalized) intensities of the GeneChips. The RMA measures were computed using the R package program, which is freely available on the web site (http://www.bioconductor.org). We then removed all genes whose maximum minus minimum values were less than 2 (2-fold change), and selected 1315 genes, which were differentially expressed between the cells during co-culture. Using the *k*-means clustering algorithm, these genes were classified into 10 clusters on the basis of similarity of their expression profiles.

2.6. Flow cytometry

The surface expression levels of FcεRI were determined as described previously [15]. For measuring the surface expression of IL-17Rs, mast cells were pretreated with 2.4G2 (BD Biosciences, San Diego, CA) were then treated with 20 μg/ml IL-17 (R&D Systems) at 4 °C for 60 min. Labeling of the cells was performed by incubation with a phycoerythrin (PE)-conjugated anti-mouse IL-17 antibody (BD Biosciences) at 4 °C for 10 min. For measuring the expression of ICAM-1, c-kit, or CD81, FITC-conjugated anti-ICAM-1, PE-conjugated anti-c-kit, or anti-CD81 antibody (BD Biosciences) was used, respectively.

2.7. Immunoblot analyses

Immunoblot analysis was performed as described previously [11] using antibodies raised against actin, $G\alpha_{i3}$ (Chemicon, Temecula, CA), $G\alpha_{i1}$, Itk (Upstate Biotechnology, Charlottesville, VA), $G\alpha_{i2}$, COX-2, GATA-1, c-Myb, Tiam1, Lyn (Santa Cruz, CA), and COX-1 (Cayman Chemicals, Ann arbor, MI).

2.8. Measurement of cytosolic Ca^{2+} concentrations

Cytosolic Ca^{2+} concentrations were measured using Fura-2/AM as described previously [11].

2.9. Purification of peritoneal mast cells

Peritoneal mast cells were purified by means of MACS system in accordance with the manufacturer's instruction (Miltenyi Biotech, Bergisch Gladbach, Germany). Briefly, mast cells were enriched using the magnet-conjugated anti-c-kit antibody after depletion of the other cell lineages using the antibodies against CD11b, CD45R, CD90, and Ter119. The purity of mast cells was greater than 98% based on the Safranin staining.

3. Results and discussion

3.1. Changes in granule staining properties, protease activities, and histamine content of cultured mast cells

We found in the preliminary experiments that the previously reported co-culture methods to develop CTMC-like cells have room for improvement in reproducibility. Since mast cells can affect growth of the feeder fibroblasts and vice versa [16], a slight change of the culture condition can lead to imbalance of the number of mast cells and fibroblasts, which often affects the process of maturation. We employed the mitomycin C treatment to exclude such instability in the co-culture system. Our method exhibited several advantages over the reported methods using 3T3 fibroblasts, in particular in terms of high reproducibility and expandability, which allowed us to investigate the changes over time. Although at Day-0, the majority of cells (>90%) were stained with Alcian blue but not with Safranin, the population of Safranin-positive mast cells was gradually increased up to ~80% at Day-16 of the co-culture (Fig. 1A). It is generally accepted that an increase in histamine content and granule protease expression reflects maturation of mast cells [17]. All the three kinds of granule protease activities and the cellular histamine content were found to be gradually increased (Fig. 1B–E). High levels of FcεRI and c-kit were detected on the surface of more than 95% of the cultured mast cells throughout the co-culture period (Fig. 1F, and data not shown).

A recent study described the generation of a large number of high-purity CTMC-like mast cells from mouse fetal skin cells [10]. Embryonic stem cell–derived mast cells have also been found to be a good model for CTMCs [18]. However, it was difficult to investigate the changes during mast cell maturation using these culture methods, since differentiation and maturation of mast cells from progenitors occurs concurrently with elimination of the other cell lineages. In contrast, we used BMMCs, the vast majority of which expresses both c-kit and FcεRI, as the initial population to develop mature mast cells. The changes observed in our system are therefore attributed solely to those in the mast cell lineage.

3.2. Gene expression profile during maturation of cultured mast cells

The characterization of the co-cultured mast cells suggested that our system reflected the process of terminal differentiation of CTMCs. We therefore performed the microarray analysis of gene expression in the cultured mast cells to gain a deeper appreciation on this process at the molecular levels. The number of genes, of which expression levels represent greater than 2-fold change, was 1315. These genes were classified into 10 groups by the clustering analysis (Fig. 2 and Supplementary data).

Expression profiles of several genes appeared to correlate well with characteristic changes concomitant with mast cell maturation. (i) The drastic induction of mast cell protease genes (*Mcpt*) is consistent with the increase in tryptic and chymotryptic activ-